8-2014

Neutron Diffraction Study of Engineering Materials Subjected to Complex Loadings

Jeffrey R. Bunn
University of Tennessee - Knoxville, jbunn3@utk.edu

To the Graduate Council:

I am submitting herewith a dissertation written by Jeffrey R. Bunn entitled "Neutron Diffraction Study of Engineering Materials Subjected to Complex Loadings." I have examined the final electronic copy of this dissertation for form and content and recommend that it be accepted in partial fulfillment of the requirements for the degree of Doctor of Philosophy, with a major in Civil Engineering.

Dayakar Penumadu, Major Professor

We have read this dissertation and recommend its acceptance:

Easo P. George, Richard M Bennett, H. Choo, Thomas R. Watkins

Accepted for the Council:

Carolyn R. Hodges

Vice Provost and Dean of the Graduate School

(Original signatures are on file with official student records.)

Neutron Diffraction Study of Engineering Materials Subjected to Complex Loadings

A Dissertation Presented for the

Doctor of Philosophy

Degree

The University of Tennessee, Knoxville

Jeffrey R. Bunn

August 2014

ACKNOWLEDGEMENTS

First I would like to express my gratitude to all those who have helped me in my research and successful completion of this dissertation. I would not be the person I am today without a professor named Bob LeMaster approaching me in 2006 asking me to be a intern with him and another student at Oak Ridge. Dr. LeMaster served as a great mentor in those times at ORNL and as a colleague still. It was also at ORNL that I met Dr. Cam Hubbard. Words are hard pressed to describe the great mentor Cam has been to me over the last eight years. Without his constant guidance I cannot see how I would have made it this far. He remains a trusted mentor and a great friend.

I am also indebted to my research advisor Dr. Dayakar Penumadu, who above all always provided me with opportunities. Dr. Penumadu provided the opportunity to be a part of his wonderful, diverse research group as well as the opportunity to pursue my Ph.D. as part of the STAIR program at UTK. He was always flexible, allowing me to choose what research I wanted.

I want to also thank the members of my graduate committee, Dr. Easo George, Dr. Richard Bennett, Dr. Hahn Choo, and Dr. Tom Watkins. Their valuable insight into my dissertation has been essential.

I also want to thank my friends in colleagues from the research group: Robin Woracek, Felix Kim, Matt Kant, Akawut "O" Siriruk, Stephen Puplampu and Ken Thomas. Also Jane Breder, Dr. Paul Frymier, Dr. David Keffer from the STAIR program.

A special thanks to my friends Rosemary Le, Travis and Kirby Russell, Paul and Laura Cutler, Paul Willard, Tihami Qureshi, Justin Roop, Dan Spencer, and Chris Morten as well as the rest of the BBM crew for their continued moral support in this long process.

Also, I want to thank my parents, as well as my siblings for their continued support.

Finally I would like to give gratitude to my wife, Sarah, for her love and moral support throughout this process. Her guidance has always been helpful and without her I would not have been able to complete this journey.

ABSTRACT

No studies using diffraction have specifically aimed to study the (*hkl*) specific shear strain of lattice planes to the application of pure shear due to applied torsion. Also no measures of strain resultant from combined loads of tension and shear stress applied simultaneously have been performed. Current techniques simply measure the planar response to axial stress and cannot provide shear strains directly. Shear moduli are not necessarily related through traditional continuum mechanics to planar Youngs' moduli (E_{hkl}) from these axial experiments for all materials. This is of significance as most engineering components fail under the influence of shear stress, or combination of shear and axial stress, rather than solely under axial stress. However, even though shear is the predominant loading case and yield mechanism, no exhaustive studies have yet been carried out describing the (*hkl*) specific shear strain in response to applied shear stress. A new technique that has been implemented as a proof-of–concept at the 2nd Generation Neutron Residual Stress Mapping Facility (NRSF2) at Oak Ridge National Laboratory (ORNL) that is able to indirectly measure the shear response of individual hkl plane. Torsion provides a unique opportunity to study the mechanical behavior of materials subjected to pure state of shear stress. An additional technique is presented that allows for the measurement of a full strain tensor in materials subjected to complex and combined proportional loads of axial and shear stresses. These new techniques are utilized to measure the planar response of a bcc ferretic steel alloy *ex situ* (post loading) and *in situ* (during loading). A comprehensive analysis of the strain tensors derived through neutron diffraction experiments on this material measured *ex situ* and *in situ* are presented. Also, a detailed description of gauge volume location through an advanced laser tracker system is demonstrated.

TABLE OF CONTENTS

LIST OF TABLES

LIST OF FIGURES

CHAPTER 1. INTRODUCTION AND SCIENTIFIC THEORY

Motivations and Overview

The given state of stress/strain within an engineering component is known to highly influence the strength of the component, as well as its useful life. In the absence of applied load, this internal state of stress/strain is referred to, in general, as residual strain or residual stress. These strains and stresses can arise through various conditions. They can result from processes during formation or can be induced after formation. Residual strain can also be either a benefit or a detriment to an engineering component. In the case of welds, it is demonstrated that tensile residual strains can accumulate along the weld bead, and these strains can effectively reduce the strength and allow premature yield through crack propagation upon the application of an external tensile force (Hutchings, Withers, T.M.Holden, & Lorentzen, 2005; Smith et al., 1988; R. Winholtz & Krawitz, 1995). Alternatively, compressive surface strains can be generated in a material to prevent crack propagation and increase the component's useful life (Webster & Ezeilo, 2001). Some common techniques for generation of compressive surface stresses in metals are shot-peening and carburization (Hutchings et al., 2005; Webster & Ezeilo, 2001).

Techniques for measurement of residual strain have been developed previously. Originally the techniques explored were destructive in nature (Ruud, 1982), which is undesirable in many cases. These techniques typically involve mounting of surface strain gauges and the drilling of a hole or cutting of a sample adjacent to the surface mounted strain gauge to relieve the residual stress within the sample (Chen & Oshida, 1989; Ruud, 1982). Alternatively an indentation can made into the surface to measure the residual stress (Suresh & Giannakopoulos, 1998). Furthermore, these destructive techniques are not always feasible and mapping the strain

is difficult due to the bulk nature of strain gauges and difficulty to achieve measurement of strains with depth.

X-ray and neutron diffraction are well-established non-destructive techniques for mapping *hkl* lattice specific strains within engineering materials (Allen, Hutchings, Windsor, & Andreani, 1985; Hutchings et al., 2005; I.C. Noyan & Cohen, 1987; J. W. L. Pang, Holden, & Mason, 1998; Withers, Preuss, Steuwer, & Pang, 2007). Each of these techniques has advantages and disadvantages. X-ray diffraction (XRD) is uniquely suited for probing near-surface strain responses and mapping residual strains. However the penetration of laboratory XRD is limited to less than 100 μm for a typical laboratory setup. For XRD to achieve a measurement at greater depth within engineering materials, electro-polishing or synchrotron radiation is required. During this polishing it is possible however to relieve internal strain by creating a free surface influence the x-ray diffraction signal, which again is undesirable. Neutron diffraction is better suited for bulk measurements within a sample. In neutron diffraction, penetration on the order of centimeters is achievable in most engineering materials. However, neutron diffraction is limited to larger gauge volumes (millimeters typically), instrument availability, and potential long term sample sequestration due to activation. Additionally, neutron diffraction can present challenges in interpretation of near surface strains due to partial filling of the neutron gauge volume.

A majority of the published experimental data associated with the lattice strain response of polycrystalline materials to applied loads has been obtained using uniaxial tensile loading (Clausen, Lorentzen, Bourke, & Daymond, 1999; J. W. L. Pang et al., 1998) . In practical applications, however, shear is often the predominant loading case and leading yield mechanism, but only a few detailed diffraction studies under direct application of shear stress or the application of complex combined proportional stress have been carried out (Marin, Dawson,

Gharghouri, & Rogge, 2008; Withers, Turski, Edwards, Bouchard, & Buttle, 2008). Shear is difficult to measure within a sample due to the fact that diffraction only measures the change in distance between atomic planes, only providing a normal strain. Shear strain requires that multiple responses are measured such that the state of strain can be used to determine the shear strain response.

An important consideration is that a strain component is best described as the vector containing the magnitude of the deformations acting on the given infinitesimal part within a body, in the direction measured. However the strain state is the collection of all of these vectors acting in 4π on the aforementioned infinitesimal point, and can be represented as a rank-2 tensor. This means that measurement of a single component will not describe the entirety of the stress/strain state. In fact, a minimum of six independent strain components must be measured, in general, to measure the state of stress/strain.

The focus of this study is to expand the methodology for measurement of residual and applied *hkl* specific lattice strains to determine of a general strain tensor. The state of general strain should be measured on both an *ex situ* and *in situ* bases, which means measured after loading and during loading respectively. From this expanded methodology, shear strains can be deduced and a greater understanding of material responses to the application of biaxial and complex proportional loadings can be formulated. The measurement techniques chosen for residual strain measurement are neutron diffraction. These methods are preferred due the ability to map conveniently individual *hkl* lattice specific responses as well as being non-destructive.

A major challenge faced when attempting to measure the general strain tensor response in a material using neutron diffraction is that a symmetric gauge volume must be used. This is required do to the fact that the gauge volume needs to be rotated about two axes to measure

multiple strain vectors. The ability to define a small, symmetric gauge volume, at the center of these two rotational axes presents additional challenges. The gauge volume defined by the incident and diffracted slits of the instrument must remain at the same point in the sample while undergoing these rotations. Also, at the minimum, the definition of a small gauge volume will lead to greatly reduced count rates; therefore the instruments used for the study must have a high flux.

Another challenge is that within a cylindrical sample subjected to a biaxial load such as pure torsion (simple shear) or a complex combined loading (both tension and torsion) the material's response will vary radially. This means that the gauge volume will contain a heterogeneous response of strain across the gauge volume. In the simpler case of uniaxial tension, the response along the gauge volume is homogeneous along the axial direction; therefore precise control of the gauge volume is not required. These challenges are magnified when expanding to *in situ* deformation studies. This is because now an entire load frame, which can provide complex loading conditions, must be included in these rotations. Alignments must be performed to repeatably place the neutron gauge volume at the desired measurement location with a great deal of precision.

Recently, neutron diffraction has made great strides to address these challenges. First, the demands for smaller gauge volumes have grown in recent years and many instruments have sufficient flux to have reasonable count times for gauge volumes of 1mm x1mm x1mm. Secondly, advanced methodologies for sample gauge volume alignment have been developed. These advanced alignment techniques include advanced optical alignment as well as even more advanced laser tracker alignment systems.

The issue of a load frame which is small enough to be placed on an engineering diffractometer yet still apply combined tension/torsion load conditions to a sample is addressed by a load frame developed at the University of Tennessee within the group of Dr. Dayakar Penumadu by the Ph.D. student Robin Woracek. The frame is uniquely designed to be able to perform complex loadings on engineering samples while still being compact enough to be mounted onto neutron instruments.

With the current level of technology at diffraction instruments, supplemented by portable stages such as the combined tension/torsion load frame from UTK, successful measurements of the *hkl* lattice specific response of engineering materials have become possible.

Bragg's Law

It was 20 years after Röntgen made his discovery of x-rays in 1896 (Röntgen, 1896) that Bragg began to convince scientists to use his novel technique to determine stress. In 1920 a number of articles were released detailing a methodology for strain determination using diffraction (Joffe, 1922; Lester & Aborn, 1925; van Arkel, 1925). Since this early development even more development of the x-ray technique has been performed. The superlative source on x-ray diffraction techniques was published by Cullity in 1956 (B. D. Cullity, 1978). The major shortfall of these instruments however was their lack of penetration into materials used in industry. Only by removing layer through polishing, etching, or machining could the technique be used to probe stresses with depth. Even in these cases, a correction is most likely required for the removal of the material that was previously constraining the measurement location.

The measurement of residual stress using neutron diffraction relies on the fundamental relationship formulated by W.H. Bragg in 1913 for utilization in x-ray diffraction (Bragg, 1913; Bragg & Bragg, 1913). Bragg formulated that a relationship existed between the wavelengths of

incoming radiation (λ) the *hkl* lattice spacing of a crystal (d_{hkl}) and the angle (θ_{hkl}) at which radiation is scattered coherently and elastically from the lattice planes. This relationship is visualized in Figure 1.1.

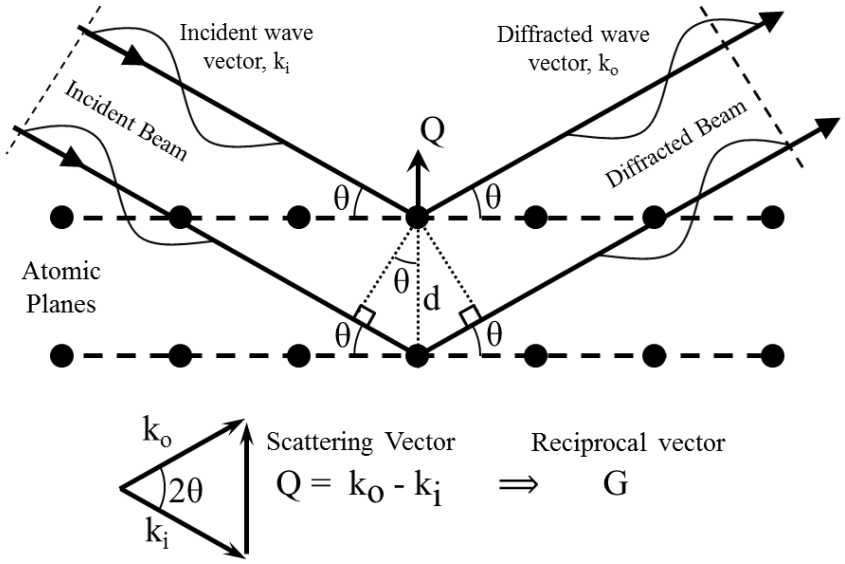

Figure 1.1 Elastic neutron scattering and Bragg's law

Bragg's proposed relationship is best represented in reciprocal space. Reciprocal space is a derivative space in which the three-dimensional array of the lattice points of a crystal lattice is defined. The basis for reciprocal space is formed by three vectors represented by $\mathbf{b_i}$. The relations to the real space lattice parameter equivalents ($\mathbf{a_i}$) is given by Equations (1.1) – (1.3) (B. Cullity & Stock, 2001)

$$b_1 = \frac{a_2 \times a_3}{a_1 \cdot a_2 \times a_3} \tag{1.1}$$

$$b_2 = \frac{a_3 \times a_1}{a_1 \cdot a_2 \times a_3} \tag{1.2}$$

$$b_3 = \frac{a_1 \times a_2}{a_1 \cdot a_2 \times a_3} \tag{1.3}$$

Orientation and regular spacing between lattice planes are given by Miller indices (*hkl*) of a lattice plane. The corresponding reciprocal lattice vector can be then defined as,

$$\boldsymbol{T_{hkl}} = h \cdot \boldsymbol{b_1} + k \cdot \boldsymbol{b_2} + l \cdot \boldsymbol{b_3} \tag{1.4}$$

Within a single crystal, $\mathbf{T_{hkl}}$ is normal to the *hkl* plane and has a length inversely proportional to the lattice spacing of the atomic planes as shown in Equation 1.5.

$$|\boldsymbol{T_{hkl}}| = \frac{1}{d_{hkl}} \tag{1.5}$$

Finally if the incoming wavelength is known (λ), the interplanar d-spacing (d_{hkl}) can be determined if the angle of diffraction (θ_{hkl}) is known. This relationship is known as Bragg's law.

$$\lambda = 2d_{hkl} \sin(\theta_{hkl}) \tag{1.6}$$

This relationship serves as the basis for measurement of planar strain, and therefore planar stress that is used in this study.

Strain Determination from Bragg's Law

Lattice specific strains in the bulk can be ascertained using diffraction. The technique has been described in detail previously. The lattice specific strain (ϵ_{hkl}) is given by the equation,

$$\epsilon_{hkl} = \left(\frac{\Delta l}{l}\right)_{hkl} = \frac{d_{hkl} - d^0_{hkl}}{d^0_{hkl}} \tag{1.7}$$

where d_{hkl} is the d-spacing measured using Bragg's Law (Equation 1.6) and d^0_{hkl} describes the stress-free reference lattice spacing (B. Cullity & Stock, 2001; Hutchings et al., 2005; I.C. Noyan & Cohen, 1986; I.C. Noyan & Cohen, 1987).

The unstressed lattice spacing can be difficult to ascertain absolutely. Many of the accepted values depend on measurements of stress free powder samples, which is sufficient for most applications. However in some complex cases the stress free lattice spacing may depend on chemistry as well as other factors not accounted for in a pure powder sample (R. LeMaster, Boggs, Bunn, Hubbard, & Watkins, 2007; R. A. Lemaster, Boggs, Bunn, Hubbard, & Watkins, 2009).

Residual Stress and Neutron Diffraction

Only in the past two decades has neutron diffraction grown to be a complimentary tool for measurement of residual stress alongside the traditional x-ray method described by Cullity. The origins of neutron diffraction can be traced to the Nobel Prize winning work of Brockhouse and Schull which occurred in 1946 at the Clinton pile reactor in Oak Ridge, Tennessee (Shull, 1995). The first experimental instruments setups for the measurement of residual stress were not reported until the 1980s despite the early prominence of neutron diffraction (Allen et al., 1985;

Krawitz, 1981; Pintschovius, 1981). Eventually the technique became established and is now an accepted method for measurement of residual stresses in the bulk of engineering materials. A definitive guide to this was published in 2005 by Hutchings et al. (Hutchings et al., 2005). Some notable contributors in the development the technique are A.J. Allen, A.D. Krawitz, M.J. Schmank, M.T Hutchings, P.J. Withers, T. Lorentzen and T.M. Holden.

Unlike laboratory XRD, the availability of neutron experimental time is very limited. The experiments must be performed at a small number of neutron sources worldwide. Additionally, the type of neutron source is very important as it will dictate the strengths/weaknesses of the diffractometer. This study is exclusively performed at a steady-state (reactor) source for neutrons.

In the case of a reactor source for neutrons, the neutrons are produced as a byproduct of the nuclear reaction. Typically research reactors have been built to exclusively produce neutrons for the purpose of study of materials. In the case of this study, the Neutron Residual Stress Mapping Facility (NRSF2) within the High Flux Isotope Reactor (HFIR) on the campus of Oak Ridge National Laboratories (ORNL) is used. In the case of HFIR, the original goal of the reactor was production of isotopes for study and medical purposes. In the 1960s HFIR was built to provide transuranic isotopes. Increasingly over the life of the facility the mission grew to irritation studies, and to neutron scattering. In 2007 a major upgrade was performed to the reactor and instrument hall to provide for increased neutron scattering capabilities (Primm, Chandler, Jolly, Miller, & Sease, 2008; Pynn, 1984).

At NRSF2, thermal neutrons are utilized, which are faster, higher penetrating and have a shorter wavelength. At HFIR, a monochromator is used to attain a preferred incident wavelength. The monochromator used at NRFS2 is a bent-crystal of silicon with a known orientation and

lattice spacing. With this information, one can use Bragg's law to select a desired wavelength from the polychromatic beam of the reactor. (Oak Ridge National Laboratory, 2009; Primm et al., 2008; Pynn, 1984)

The general layout of NRSF2 is shown in Figure 1.2. The detector assembly uses a series of seven linear He-3 detectors. The detectors are placed such that multiple peaks along the Debye-Scherrer cone can be measured. The instrument stages, monochromatic and detector are all identified.

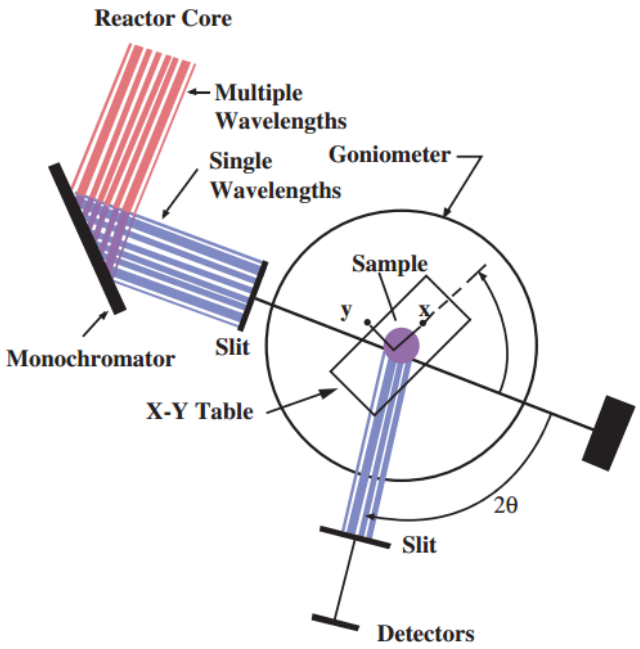

Figure 1.2 Instrumental setup at NRSF2 (R. A. Lemaster et al., 2009)

At neutron diffraction, the beam is defined by slits and the intersection of these slits will define a measurement gauge volume. A sketch of a typical diffraction setup is illustrated in Figure 1.3. Bisecting the incident and diffracted beams is the diffraction vector, Q. The diffraction vector defines the direction of d-spacing and therefore strain that is being measured in the current experimental orientation. It is important to note that within a polycrystalline material

only the grains which have planes that are aligned such that Bragg's law is satisfied and are within the probed gauge volume will contribute to diffraction. These grains are highlighted in red in Figure 1.3 for clarity.

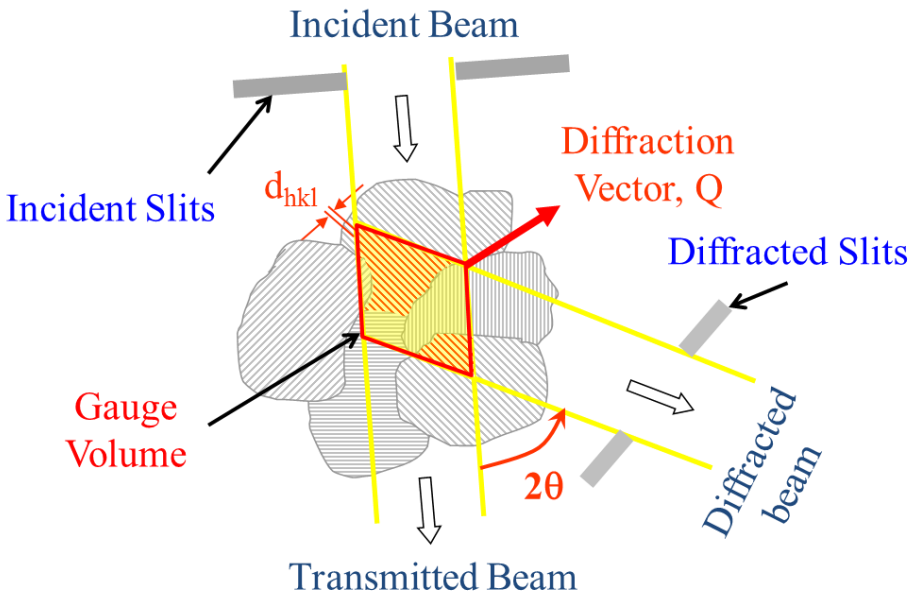

Figure 1.3 Sketch detailing diffraction on polycrystalline material

Strain Tensors

The state of strain (in general) is described as the totality of all the strain components at that point, and is represented by a rank-2 symmetric tensor. The strain tensor ϵ_{ij} has six independent components due to symmetry, in a right hand Cartesian coordinate system is expressed by:

$$\varepsilon_{ij} = \begin{bmatrix} \epsilon_{11} & \epsilon_{12} & \epsilon_{13} \\ \epsilon_{21} & \epsilon_{22} & \epsilon_{23} \\ \epsilon_{31} & \epsilon_{32} & \epsilon_{33} \end{bmatrix} \tag{1.8}$$

where ϵ_{11}, ϵ_{22}, and ϵ_{33} are the normal strain components. ϵ_{12}, ϵ_{21}, ϵ_{13}, ϵ_{31}, ϵ_{23}, ϵ_{32} represent the shear strain components and $\epsilon_{12} = \epsilon_{21}$, $\epsilon_{13} = \epsilon_{31}$, $\epsilon_{23} = \epsilon_{32}$.

A majority of studies only consider a single component response of strain or measure three directions which are geometrically normal, and convenient to measure within a given sample. An example of this would be measuring the axial, hoop (circumferential), and radial directions in a cylindrical sample. The critical flaw with this assumption is that these three geometrically normal strains are not necessarily the principal strains. This assumption is not valid when exploring samples subjected to pure torsion or a combined proportional loading of tension and torsion.

To fully measure the response to a system exposed to a complex or biaxial state of loading, the strain tensor needs to be mapped. From a tensor, one can deduce the principal strains' magnitudes, directions, as well as the strain component in any desired direction. The maximum, intermediate, and minimum principal strains are represented by ϵ_1, ϵ_2, ϵ_3 respectively. The maximum principal strain, ϵ_1, is defined as the greatest normal strain in which all shear strain is zero. Similarly, the minimum principal strain, ϵ_3, is the smallest normal strain is which all shear strain is zero. And lastly the third strain, ϵ_2, is defined at the intermediate strain and will satisfy $\epsilon_1 > \epsilon_2 > \epsilon_3$ (Dieter, 1986; Eringen, 1980; Malvern, 1969; Mase, 1970).

A tensor also yields invariant information. Invariants are values that remain constant for any rotation of the tensor. Von-Mises yield criteria for example, is heavily used in predicting yield of a material and is the focus of many finite element modeling efforts for engineering applications. This yield criterion relies on the J_2 invariant of the symmetric stress tensor (Dieter, 1986; Ford, 1963; Hill, 1950; von Mises, 1913).

Another important invariant is the octahedral shear strain invariant. This value is an additional invariant of a rank-2 tensor and will serve as a basis for comparison of the stress paths. The octahedral shear strain is defined as:

$$\gamma_{oct} = \frac{2}{3}\sqrt{(\epsilon_{11} - \epsilon_{22})^2 + (\epsilon_{22} - \epsilon_{33})^2 + (\epsilon_{33} - \epsilon_{11})^2 + 6({\epsilon_{12}}^2 + {\epsilon_{23}}^2 + {\epsilon_{13}}^2)} \quad (1.9)$$

Height-Westergaard space (also referred to as stress space) is a 3-dimensional space in which the three axes represent the three principal strains experienced in a deformed body. Within that space various yield surfaces can be represented graphically. In the case of a ductile metal, a von Mises criterion is common (Hill, 1950). A graphic detailing Height-Westergaard space including the von Mises yield surface (light blue cylinder) is shown in Figure 1.4. Also it is convenient at times to display the results in various 2-D projections of Height-Westergaard space for clarity. The von Mises criterion assumes yield is independent of hydrostatic strain/stress (all principal stresses equal); therefore a common approach is to explore the deviatoric plane. The deviatoric plane is a 2-D plane derived from the projection along the hydrostatic axis and is shown in Figure 1.4 (light green plane). In the deviatoric plane the von Mises yield is simply represented by a circle, and not a cylinder (Dieter, 1986; Hill, 1950). Also to better represent the triaxial response in 2-D, a 2-D plane where the dependent axis is coincident with the maximum principal strain axis, ϵ_1, and the independent axis is the vector that lies in the plane normal to the ϵ_1 axis and bisects the ϵ_2 and the ϵ_3 axes.

The triaxial plane (also referred to as the radially symmetric or R.S. plane) is shown in Figure 1.4 as a red plane. Within this plane the projection combines the ϵ_2 and ϵ_3 axes into a single axis in which $\sqrt{2}\epsilon_2$ is equal to $\sqrt{2}\epsilon_3$.

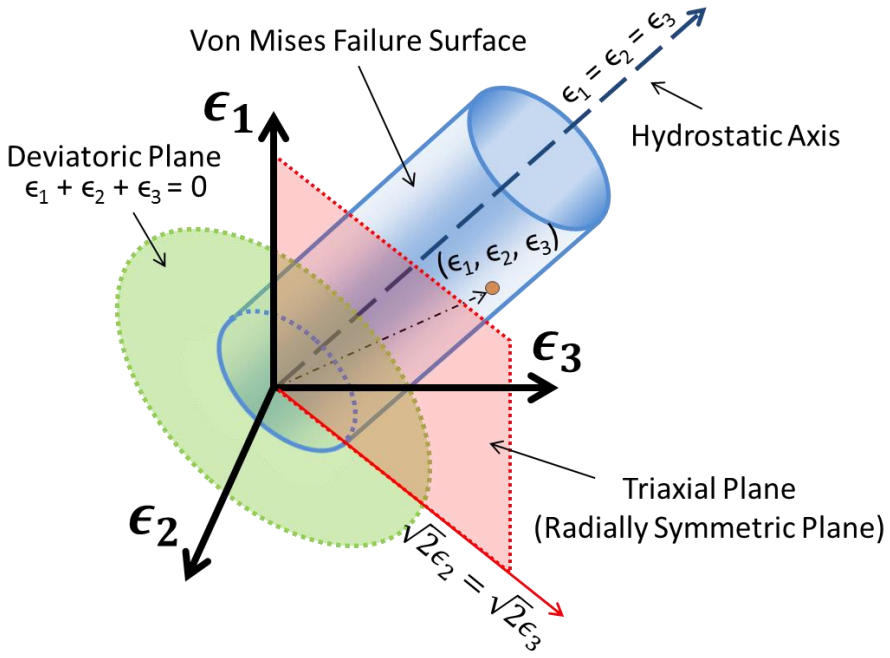

Figure 1.4 Graphic describing Height-Westergaard space (stress space)

Generalized Least Squares Method to Determine a Strain Tensor

Winholtz and Cohen established a technique to measure a strain tensor (full state of strain) from a series of neutron diffraction measurements (R. A. Winholtz & Cohen, 1988). In the technique, a minimum of six independent strains must be measured by rotations of the sample about the center of the gauge volume. This technique is critical in this study of complex and proportionally loaded materials.

In the technique, two coordinate systems are considered and are shown in Figure 1.5. The sample coordinate system (S) is based upon the sample and the coordinate system in which the desired strains are located. A second coordinate system (L) is the laboratory coordinate system, this is the system that in which the diffraction measurements are obtained. The two coordinate

systems are related by two angles ϕ and ψ. If the unstressed lattice spacing (d^0_{hkl}) is known, and the d-spacing of planes perpendicular to the L3 direction, $d_{\phi\psi}$, are measured then using Equation 1.10 the strain $\epsilon_{\phi\psi}$ can be determined.

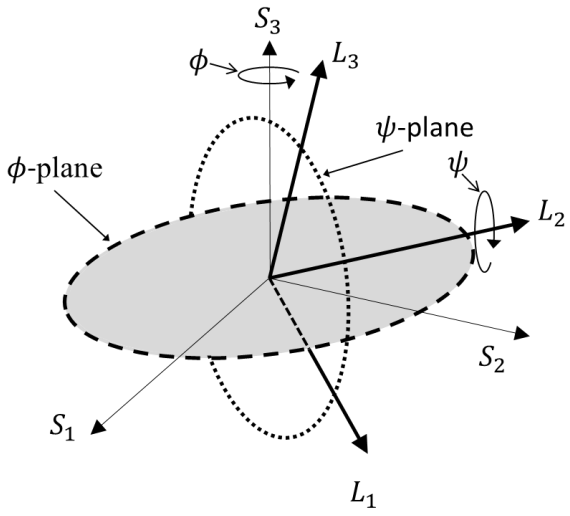

Figure 1.5 Relationship between the laboratory (L) and the sample coordinate systems (S)

$$\epsilon_{\phi\psi} = \frac{d_{\phi\psi} - d_0}{d_0} \tag{1.10}$$

Noyan has previously derived a relationship between the components of the rank-2 symmetric strain tensor (Equation 1.8) and the derived strain $\epsilon_{\phi\psi}$. This relationship is:

$$\epsilon_{\phi\psi} = \epsilon_{11}\cos^2\phi\sin^2\psi + \epsilon_{22}\sin^2\phi\sin^2\psi + \epsilon_{33}\cos^2\psi + \epsilon_{12}\sin 2\phi\sin^2\psi + \epsilon_{13}\cos\phi\sin 2\psi + \epsilon_{23}\sin\phi\sin 2\psi, \tag{1.11}$$

where ϵ_{ij} refers to strains in the sample coordinate system strain tensor.(R. A. Winholtz & Cohen, 1988)

A minimum of six combinations of ϕ and ψ are required for measurement of a complete strain tensor. In practice, many more points are taken and a least squared analysis is performed. The process of the least squared analysis beings with a matrix formation based on Equation 1.11. The matrix formed is:

$$\begin{aligned}
\epsilon_1 &= \epsilon_{11}, \qquad f_1(\phi,\psi) = \cos^2\phi \sin^2\psi\,,\\
\epsilon_2 &= \epsilon_{22}, \qquad f_2(\phi,\psi) = \sin^2\phi \sin^2\psi\,,\\
\epsilon_3 &= \epsilon_{33}, \qquad f_3(\phi,\psi) = \cos^2\psi\,,\\
\epsilon_4 &= \epsilon_{12}, \qquad f_4(\phi,\psi) = \sin 2\phi \sin\psi\,,\\
\epsilon_5 &= \epsilon_{13}, \qquad f_5(\phi,\psi) = \cos\phi \sin 2\psi\,,\\
\epsilon_6 &= \epsilon_{23}, \qquad f_6(\phi,\psi) = \sin\phi \sin 2\psi.
\end{aligned}$$

The residual between the measured and calculated strain along the L3 vector can be represented by the equation:

$$r_i = \sum_{j=1}^{6} \epsilon_j f_j(\phi_i,\psi_i) - \epsilon_i \qquad (1.12)$$

Building upon Equation 1.12, the total weighted sum of the squared error, R, for *n* number of strain measures is described by the equation:

$$R = \sum_{i=1}^{n} \frac{1}{var(\epsilon_i)} \left\{ \left(\sum_{j=1}^{6} \epsilon_j f_j(\phi_i,\psi_i) \right) - \epsilon_i \right\}^2 . \qquad (1.13)$$

By weighting each error, r_i, by the inverse of the variance, the values with the lowest variance are weighted more. The weighting of the more reliable data helps to reduce error in finalized dataset.

Next, the partial derivatives with respect to each strain, ϵj, are taken. These derivatives are then set equal to zero to find the minimum results in the set of equations. This is shown in Equation 1.14.

$$\sum_{i=1}^{n}\left\{\left(\sum_{k=1}^{6}\epsilon_k f_k(\phi_i,\psi_i)\right)-\epsilon_i\right\}\frac{f_j(\phi_i,\psi_i)}{var(\epsilon_i)}=0 \qquad (1.14)$$

To formulate a matrix equation for determination of strain the matrix **B** and the vector **E** are defined as:

$$\boldsymbol{B}_{jk}=\sum_{i=1}^{n}f_j(\phi_i,\psi_i)f_k(\phi_i,\psi_i)/var(\epsilon_i) \qquad (1.15)$$

$$\boldsymbol{E}_j=\sum_{i=1}^{n}\epsilon_i f_j(\phi_i,\psi_i)/var(\epsilon_i) \qquad (1.16)$$

Therefore through a simple Hook's Law relationship:

$$\boldsymbol{B}\epsilon_{ij}=\boldsymbol{E} \text{ or } \epsilon_{ij}=\boldsymbol{B}^{-1}\boldsymbol{E}, \qquad (1.17)$$

the strains are solved for which give the least squared error. This is of course only true as long as the **B** matrix is non-singular.

A MATLAB code is written to perform the least squared analysis of the measured data. This code is based on and validated against an earlier FORTRAN version written by Winholtz et

al. This new code has features that enhance reduction including visual graphic data analysis as well as greater availability for use by the community.

Portable Tension and Torsion Capable Load Frame

A portable mechanical loading system has been designed for the usewithin neutron diffraction and imaging beam lines. It is small in size, which is ideal for mounting onto an engineering diffractometer. Figure 1.6 illustrates the frame mounted onto NRSF2, and shows the position and direction of the incident and diffracted beams in relation to the sample and load frame. The frame is able to apply axial deformation, torsional deformation or a combination of the two simultaneously. The frame offers an axial force capacity of 0-50 kN and a torque range of 0–12 Nm. The system offers a custom control system in which the applied loads can be controlled in a combination of axial deformation control, twist control, axial stress control and maximum (surface) shear stress control.

A primary advantage of the portable load frame is that it's small size and weight allows for it to be mounted onto the NRSF2 diffractometer at an incline. This is necessary to obtain d-spacings for the generalized least squared method. Without this ability the only strain that could be measured would be $d_{\phi\psi}$ with $\psi = 90$ (upright) or $\psi = 90$ (Q along axis of tensile loading). This data alone would not form enough of a basis for determination of the 3D general state of strain within a sample.

Figure 1.6 The portable load frame mounted at an incline on the NRSF2 diffractometer.

This control system of the frame allows it to be operated independently of the neutron diffraction instrument. However, for extended measurements it is required that the system is integrated into the diffraction instrument controls. This was achieved at both NRSF2 at ORNL and the SMARTS instrument at Los Alamos National Laboratory (LANL). The greatest level of integration is at NRSF2. The controls in each were integrated such that the beamline instrument control system could send commands for the frame to drive to a specific axial deformation or axial stress and specific torsional twist or shear stress.

Due to the extremely small gauge volumes used in the study (1 mm x 1mm x 1mm) the count times were on the order of minutes, but entire runs would last hours. To achieve an accepted fidelity over the long runs needed, this integration was necessary.

Sample Material Considerations

For an experiment to yield useful data using the techniques in this study, the neutron gauge volume needs to remain fully buried within the sample during loading, unloading and rotations. Allowing the gauge volume to move outside of the sample will lead to artificial shifts of the resultant diffraction response. This issue is due to the fact that in a neutron diffractometer geometry, the center of the gauge volume is assumed to the center of diffraction. However as shown in Figure 1.3 previously, only the grains which are aligned for diffraction will contribute to the diffraction signal. Therefore the centroid of the grains contributing to diffraction is the actual center of diffraction and the empty space outside the sample surface is of course not contributing to diffraction.

This effect has been explored previously by Wang, et al (Wang, Spooner, & Hubbard, 1998). As the gauge volumes moves outside of the material as seen in Figure 1.7, the measured d-spacing will shift (From Wang, et.al). However, this shift is not real and can be misleading.

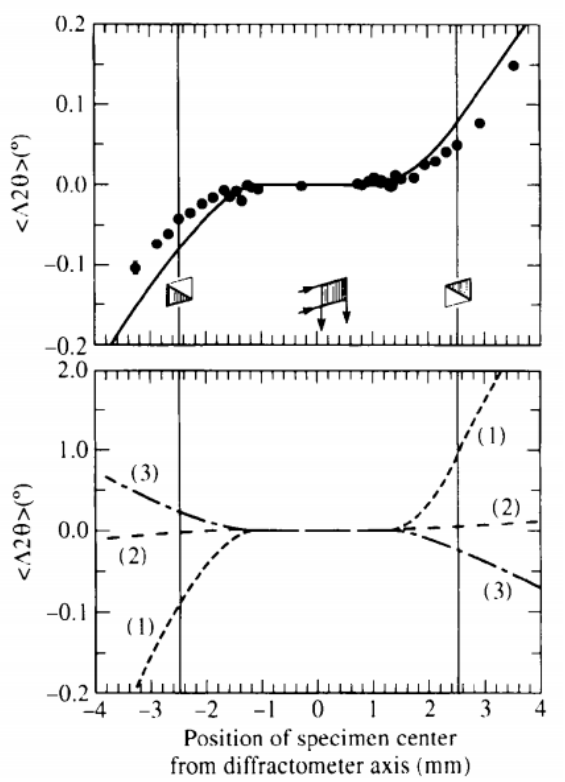

Figure 1.7 Data (from Wang et al) showing effect of partially buried gauge volumes and apparent shift in measured d-spacing (Wang et al., 1998)

A correction for the partially buried gauge volume geometries that can exist in near surface measurements has been developed previously (Taran & Balagurov, 2012). By use of this correction, the ability to measure near surface d-spacing is allowed. However this correction still makes the assumption that all the material exposed to the incoming neutrons are contributing to diffraction.

As discussed previously, engineering diffractometers define a volume of grains in a polycrystalline material over which an average response is measured. The typical size of these gauge volumes is on the order of millimeters. During the diffraction experiment, a signal is only measured for the grains which satisfy Bragg's law (perpendicular to the diffraction vector, Q).

The assumption made by diffractometers is that the center of diffraction (COD) is located at the same point as the center of the gauge volume (COGV). The center of diffraction for a fine grained isotropic material is best represented by the centroid of the expose material (Wang et al., 1998).

Ideal materials for residual stress characterization are isotropic, contain little porosity, small grained (in comparison to gauge volume size), and contain a minimum of texture. Figure 1.8a is a sketch that shows what this ideal material measured would resemble in 2D. In this case, the grains that satisfy Bragg's law are evenly distributed across the gauge volume and the COD and COGV are coincident.

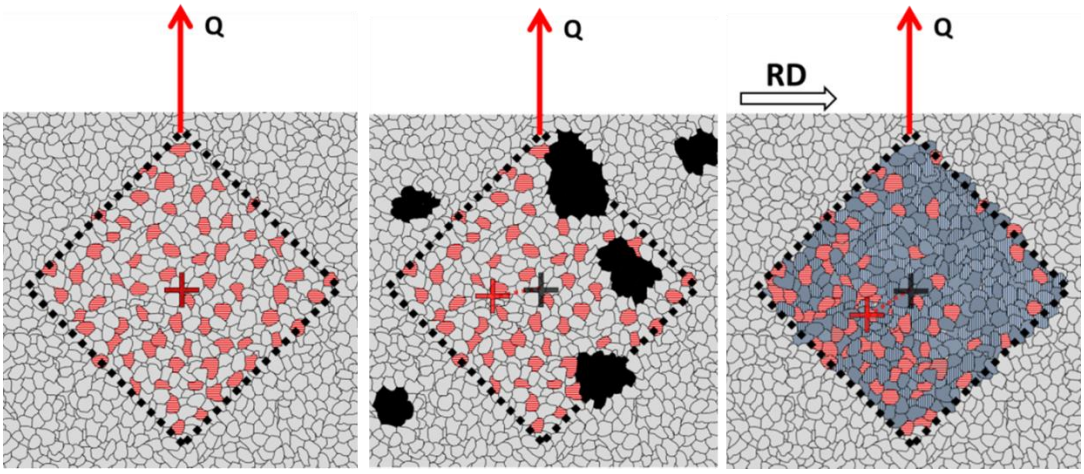

Figure 1.8 a) an ideal experimental gauge volume bounded by the black dotted line and b) a gauge volume that will experience an artificial shift due to porosity and c) a gauge volume that will experience an artificial shift due to texture.

In practice, many engineering materials contain porosity and/or texture. This can lead to a non-uniform distribution of grains contributing to diffraction. Figure 1.8b represents a gauge

volume with porosity contained within the gauge volume non-uniformly. This non-uniform distribution leads to a shift between the COGV and the COD. This shift of the center of diffraction leads to a misinterpretation in measured 2θ for Bragg peaks. A similar effect can result from texture as seen in Figure 1.8c. This shift in a textured material can still exist even when no empty space is within the gauge volume. In the case of texture this effect can be dependent on temperature and applied stress. The severity of this artificial shift in 2θ will also vary depending on the individual instrument parameters and geometry.

These considerations are extremely important in the measurement of residual stress. Because this study primarily concerns the establishment of new measurement techniques the material selected was a simple bcc iron. This choice was specifically made to mitigate any material based complications that could arise due to the aforementioned effects of porosity and texture.

Sample Alignment

Sample alignment using an engineering diffractometer is critical to controlling the placement of a small gauge volume at a desired location, particularly when performing the rotations of ϕ and ψ detailed previously. In Typical strain mapping experiments at NRSF2, an optical theodolite system is used for gauge volume placement within the sample at various measurement locations (Figure 1.9). A system of three optical theodolites can align the incoming beam of neutrons over the center of rotation with an accuracy of roughly 300μm. This level of accuracy and precision is sufficient for most applications, but as the sample and load frame are rotated out of the plane of diffraction the ability to align a gauge volume repeatedly is no longer accurate enough or preformed with enough precision over all the ψ frame rotations for the purpose of this study.

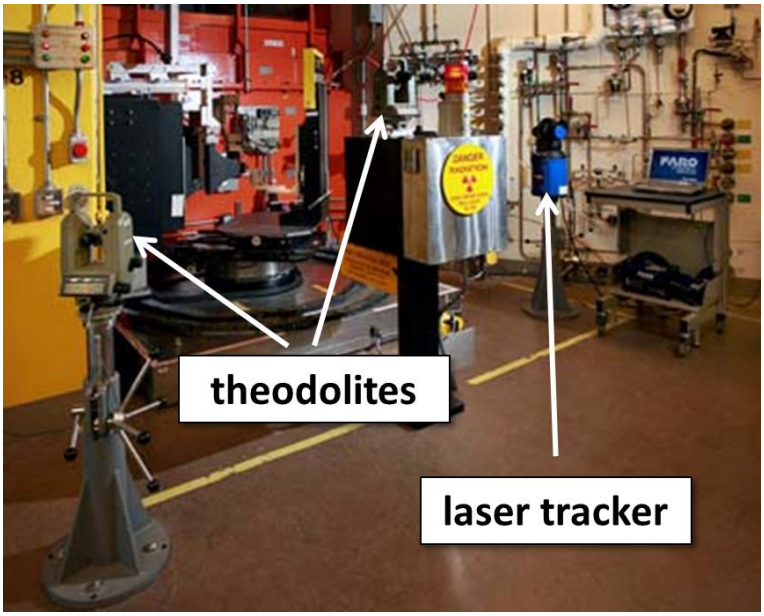

Figure 1.9 Picture of the NRSF2 facility (Oak Ridge National Laboratory, 2009)

This concern is addressed at NRSF2 using a laser tracker system combined with specialized alignment software. The system uses a laser tracker (Figure 1.9) that targets spherically mounted retro-reflectors (SMRs). The SMRs are used to define a basis, virtually, for the instrument coordinate system (ICS). Desired measurement points are defined in an established sample coordinate system (SCS). The advantage of this approach is that the points can be established based on the sample features. Off the neutron diffractometer, the sample coordinate system is established using a separate laser tracker. Fiducial points are taken by placing an SMR into a magnetic nest that is mounted onto the load frame. A series of these nests are mounted onto the load frame. The SMR is used in conjunction with the laser tracker to take coordinates for these points in the defined sample coordinate system. Next, the load frame is mounted onto the instrument in a tilted orientation. The laser tracker is used to measure the points again on the instrument in the previously defined instrument coordinate system.

Once the points are known in both the instrument and sample coordinate system, the data is entered into a special program, SScanSS. The SScanSS software utilizes a virtual instrument which can predict collisions, estimate count times, ensure the gauge volume remains buried, and orient the sample for specific diffraction vectors under rotations of the gauge volume within the sample. This software has been specially developed along in collaboration between multiple engineering diffractometers and Dr. Jon James at Open University. The program allows for definition of a sample geometry and desired measurement points. The software then performs a coordinate system transformation based on the two sets of defined fiducial points and will then provide the coordinates for the measurement points in the instrument coordinate system. This process is extremely repeatable and can be used multiple times at various tilts in the ψ rotation out of the plane of diffraction (J. A. James et al., 2008; J. A. James, Santisteban, Edwards, & Daymond, 2004).

Chapter Research Objectives

This study seeks to develop and use advanced neutron and x-ray scattering techniques to investigate engineering materials subjected to biaxial, complex, and combined proportional loading regimes on both an *ex situ* and *in situ* basis. The major objectives of this study are synopsized into the follow chapters.

In chapter 2, the traditional methodology of neutron residual stress measurement is performed on samples subjected to large plastic deformations through two different load paths *ex situ*. The first sample is subjected to uniaxial tension through axial deformations while the second is subjected to simple shear through pure torsional deformations. The two deformed samples are mapped and compared to an as-received sample and a powder reference. The traditional mapping demonstrates how specific planes are sensitive to formation of intergranular

strains under pure tension. However, the samples subjected to pure shear do not exhibit the same behavior. This had not been demonstrated previously in a polycrystalline material. This work has been published previously by the author in Applied Physics A under the title "Residual strain evolution in steel samples: tension versus torsion."

In chapter 3, the first experiments are performed where a full residual stress tensor is measured on samples subjected to different load paths. The samples used in the chapter 2 study were re-employed. To perform the measurements, an order-of-magnitude advancement in instrument alignment is identified. Through initial use of a laser tracker system and the SScanSS software, the alignment is achieved. With the full tensor response, it is clear that different *hkl* crystallographic planes respond fundamentally different to dissimilar paths of plastic deformation (uniaxial tension versus torsion). Some planes demonstrate a dependence on applied load path while others do not. This work has also been published previously by the author in Metallurgical Transactions A under the title "Effect of Multi-Axial Loading on Residual Strain Tensor for 12L14 Steel Alloy."

In chapter 4, a new method to determine an *hkl* crystallographic strain response in materials subjected to simple shear through pure torsion is demonstrated. Also, the first measurements of *in situ* neutron diffraction measurement of *hkl* shear strains under load, and the determination of elastic (*hkl*) shear moduli are reported. Multiple crystal planes are observed, results reported and compared to polycrystalline models. Differing levels of anisotropy are observed in samples subjected to shear compared to those exposed to tensile loading. This work has been jointly published previously in an abridged version in Applied Physics Letters under the title "Method to Determine hkl Strains and Shear Moduli Under Torsion Using Neutron Diffraction"

Chapter 5 is the combination of all the methodologies and knowledge that has been accumulated thus far to obtain a first-ever full strain tensor *in situ* on a sample subjected to simultaneous tension through axial deformation and shear through applied torsion. The preliminary results are to provide a proof of concept measurement to show not only the measurements are possible, but that with increased knowledge of the full stress state, materials with complex loading can be explored for future advanced material design and utilization.

Chapter 7 is a summary of the work presented, and presents future work to be explored.

CHAPTER 2. RESIDUAL STRAIN EVOLUTION: TRADITIONAL METHODOLOGY

Abstract

Torsion provides a unique opportunity to probe mechanical behavior of materials subjected to pure state of shear stress. In this research, identical steel alloy (12L14) hollow cylinder samples are subjected to predetermined amounts of plastic axial and shear strain such that their octahedral shear strain (an invariant) are identical for comparison. Measurements were made at the residual stress measuring facility at the High Flux Isotope Reactor in Oak Ridge (NRSF2), using a small gauge area in the direction of strain gradients (0.5mm x 0.5mm) through the hollow cylinder wall thickness. These orthogonal strains are obtained for BCC Fe for three hkl's. Three normal strains in the hoop, radial, and axial directions are obtained as a function of centroid position of the gauge volume through the 2mm wall thickness. Significant differences in measured residual strains are noted between the torsion and the tension samples. The largest differences are found for the Fe (200) planes while the smallest differences are observed for the Fe (211) planes. This research demonstrates the need for a systematic study of residual strain as a function of applied stress path moving beyond tensile testing for solving real world problems.

Introduction

The creation of intergranular strains during the onset of plastic deformation can lead to misinterpretation of residual strain data for samples with a history of plastic deformation (Hutchings et al., 2005). Some studies have illustrated the use of in situ studies to determine the effect of intergranular strain on residual strains using neutron diffraction measurements (Daymond & Priesmeyer, 2002). Pang has demonstrated the dependency of residual strains in various hkl planes of a steel alloy with a history of plastic deformation (J. Pang, Holden, Wright, & Mason, 2000; J. W. L. Pang et al., 1998). Some planes are stated to be weakly affected by

intergranular strains and others are said to be strongly affected by intergranular strains. Hutchings asserts that residual strains in the Fe (110) and Fe (211) planes are weakly affected by intergranular strains while the Fe (200) is strongly affected (Hutchings et al., 2005).

The measurement of residual strain in a deformed steel alloy in Pang's experiment was limited to those caused by tensile mode of deformation. To the authors knowledge, the effect of torsion on residual strain evolution has not been studied in the past using neutron diffraction, except for a previous unpublished study by D. Penumadu. Torsion provides the ability to study the behavior of material subjected to pure shear deformation. This study investigated the effect of stress path (torsion versus tension) on residual stress evolution using hollow steel samples subjected to plastic deformation for hkl planes stated to be weakly and strongly affected by intergranular strains (Hutchings et al., 2005).

Residual strains in steel samples subjected to pure axial deformation were mapped spatially at locations through the wall thickness. An identical sample was also subjected to pure shear deformation using a torsional shear testing system and spatially mapped in the same manner as the axially deformed sample. At each measurement location residual strains in the axial, radial, and hoop direction were measured. Both samples were stressed to the same octahedral shear strain invariant to provide a rationale for comparison. The samples were all made from the same 12L14 BCC steel alloy and pre-loading configuration was identical including testing system, initial specimen geometry, and gripping procedures. The hot rolled and cold drawn hollow cylinder samples would exhibit residual strains from the forming process as well as potential elongation of the grains along the drawn direction. A third identical hollow steel cylinder which was not deformed was also studied to provide a benchmark of the residual strain in the samples during their forming process.

Experimental Procedure

The neutron diffraction measurements were obtained using a 2nd Generation Neutron Residual Stress Mapping Facility (NRSF2) at the High Flux Isotope Reactor (HFIR) at ORNL. The details of this instrument have been given previously.

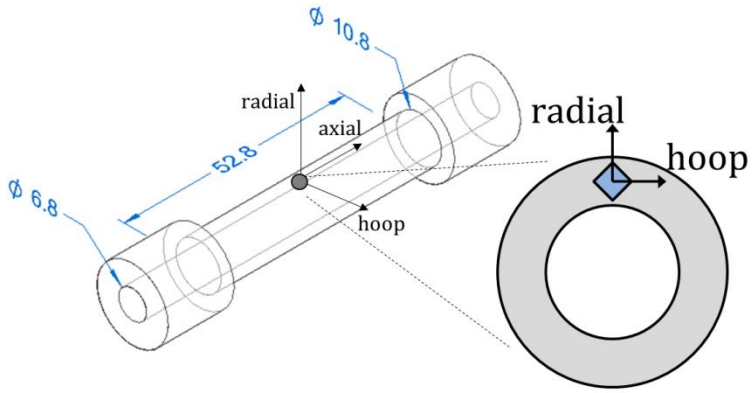

Figure 2.1. Geometric information of the samples used in diffraction studies.

All samples measured were hollow cylindrical specimens as shown in Figure 2.1 made of 12L14 steel alloy. The alloy has a single phase bcc structure, although inclusions could be expected at grain boundaries due to precipitates. The tension sample was subjected to pure axial deformation using a combined axial-torsional testing system. An additional torsion specimen was subjected to pure shear deformation using the same testing system as in the case of tensile samples using hydraulic grips and identical grip pressure.

Each sample was loaded beyond yield, and the tension and torsion samples were subjected to identical octahedral shear strain invariants. The macro axial stress-strain history and shear stress-strain history for both the tension and the torsion samples used in this study are shown in Figure 2.2. For interpreting average shear strain from measured rotation value and

average shear stress from applied torque, an assumption that the work done by the external forces (torque) is equal to the sum of the work done by internal stresses and strains involved was used. The average shear strain is given by Equation 2.1.

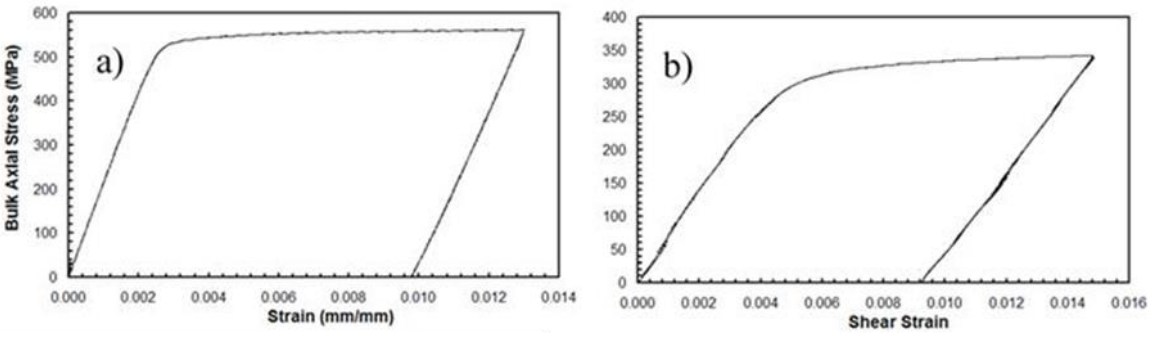

Figure 2.2 a) The axial stress-strain history to which the tension sample was subjected and b) the shear stress-shear strain history to which the torsional sample was subjected.

$$\epsilon_{\theta z} = \frac{2\theta\left(R_o{}^3 - R_i{}^3\right)}{3H\left(R_o{}^2 - R_i{}^2\right)} \tag{2.1}$$

where R_o and R_i are the outer and inner radius of the sample respectively. The twisted angle in radians is given by θ and H describes the gauge height of the sample which is subjected to torsion. The unstressed sample was subjected to no additional axial or shear deformations and was used to obtain a reference value of d-spacing of a given *hkl* at a target gauge volume location. This lattice spacing would represent the d-spacing of a sample prior to being deformed.

Residual strains in a bulk sample can be ascertained by neutron diffraction. This technique has been discussed in detail previously. The lattice strain of the desired reflection (*hkl*), ϵ_{hkl}, is determined from Equations 1.7 and 1.6,

Residual strains were measured for the Fe (110), (211), and (200) planes at five locations spatially along the wall thickness of the specimens (Figure 2.3). Table 2.1 contains information associated with the monochromator used, expected $2\theta_{hkl}$, and the neutron wavelength, λ, for each specific plane (*hkl*) used in this study.

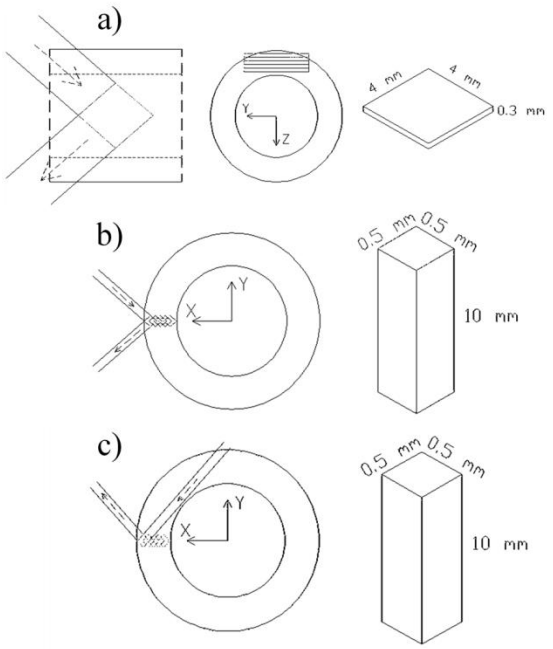

Figure 2.3 Experimental setup for measuring the strain directions and the gauge volumes used: a) axial, b) radial, and c) hoop, with mapping along the X.

All diffraction strain measurements are defined relative to a reference value of stress-free condition. This is referred to as a "stress-free approach." Many different accepted methods exist for defining stress free lattice spacing, d^0_{hkl} (Allen et al., 1985). One accepted method of obtaining the initial value of lattice spacing is to measure a surrogate stress-free powder sample.

This method was used to obtain d^0_{hkl} for each of the reflections. The powders were prepared by filing. The values obtained for d^0_{hkl} are shown in Table 2.2.

A second approach was also used to determine the stress free lattice spacing. In the "initial state approach" the measured d-spacings obtained from the sample that was not subjected to any additional plastic deformation were used as the d^0_{hkl} in the strain calculations. The strains obtained are therefore residual strains that resulted from the axial or shear deformation seen in the two deformed samples respectively. This approach will be investigated separately than the stress free approach described earlier and will give additional insight into the residual strains resulting from the deformation of the samples.

Table 2.1 Table listing instrument 2θ for each reflection investigated.

Reflection	**2θ**	**Monochromator**	**λ (Å)**
Fe (211)	95.37°	Si 331AF	1.72858
Fe (110)	82.23°	Si 220	2.66620
Fe (200)	82.54°	Si 400	1.88064

Table 2.2 Measured initial stress free lattice spacing for powder sample.

Reflection	**Initial lattice spacing, d^0_{hkl} (Å)**
Fe (211)	1.1705 ± 0.0001
Fe (110)	2.0253 ± 0.0001
Fe (200)	1.4342 ± 0.0001

Strains were characterized in the axial, radial, and hoop directions. In both the radial and hoop directions, a 0.5mm x 0.5mm x 10mm gauge volume was used. The tall and narrow gauge volume was used to decrease measurement time and still provide us with higher flexibility to measure along the direction of high strain gradients. In the axial case a flat 4mm x 4mm x 0.3mm gauge volume was used. The flat gauge volume for axial strains was chosen to preserve the 0.5mm spatial resolution while not increasing measurement time. The gauge volume was not fully buried in the sample for all measurements of the axial direction. Studies of the effects of partially buried gauge volumes have been conducted in the past [8]. These studies have shown that for gauge volumes entering samples in a plane parallel to the diffraction vector can result in a systematic shift of the measured 2θ. For the axial strains, due to the sample x-axis being perpendicular to the plane of diffraction, no systematic shift in d-spacing occurs due to partial filling of the gauge volume and no correction is required. Diagrams of the axial, radial and hoop setups and the gauge volume associated with each are shown in Figure 2.3a, Figure 2.3b and Figure 2.3c respectfully.

For the radial and hoop cases great care was taken to ensure that the full gauge volume was within the sample. Unlike the axial case, partial filling of the gauge volume would lead to a systematic shift in the d-spacing because the direction of the entering of the gauge volume is in the plane of diffraction. First theodolites were used to optically locate the outer surface of the sample. Next, neutron edge scans were carefully performed to accurately determine the outer surface. Between each sample, the reference powder was measured to ensure no environmental changes over the time of the measurement had any effects on the data.

Results

Data Fitting and Processing

All fittings were fit with a Gaussian fit. The profiles obtained for the reference powder were much broader than the profiles obtained for the specimens. The full width – half maximum (FWHM) values for the powder samples were larger than the FWHM values for the undeformed sample. This result of a larger FWHM was repeatable however, giving confidence to the validity of the d^0_{hkl} measured from the powder as well as the undeformed sample.

Stress-Free Approach

For the Fe (211) reflection, large measured residual strain gradients were observed. All three samples exhibited similar trends from the outer surface of the hollow cylinder to the inner surface through the 2 mm wall thickness (Figure 2.4). In the axial (Figure 2.4a) and radial (Figure 2.4b) case a change of 800 microstrain is observed from the outside surface to the inside diameter (I.D.). The least change in strain through thickness in the (211) reflection was noted in the hoop direction (Figure 2.4c). Slight variations of strain occur from sample to sample in the hoop direction but most are within the expected error of the measurement.

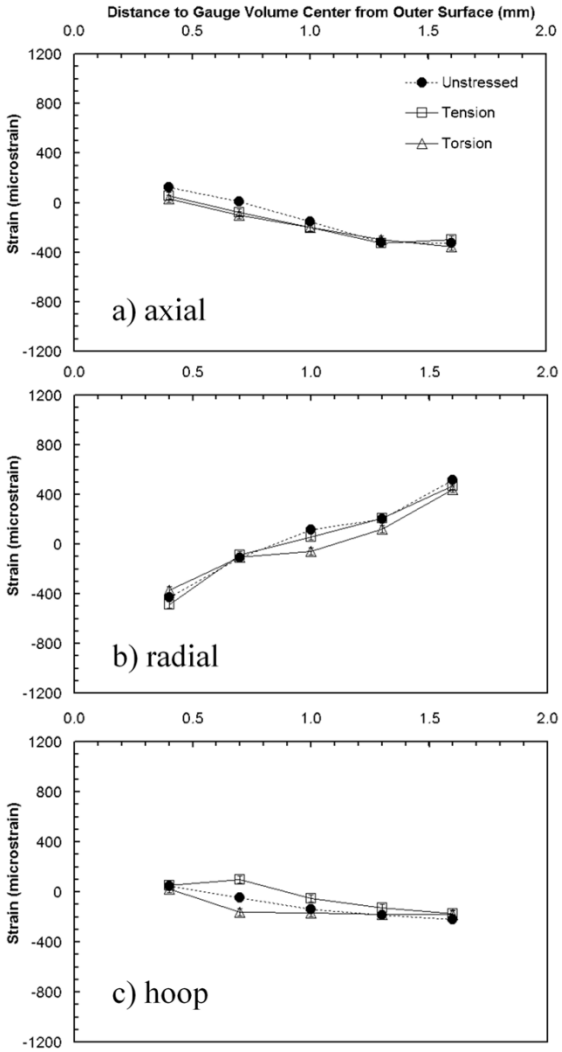

Figure 2.4 Residual strains using Fe (211) plane for the (a) axial, (b) radial, and (c) hoop directions as a function of distance from the outer surface of the hollow cylinder sample, the error shown is two standard deviations of the strain.

For the Fe (110) reflection residual strains measured in the three directions respectfully are shown in Figure 2.5. In the axial direction, the residual strains show very large differences between samples as seen in Figure 2.5a. The tension sample exhibits greater compressive residual strain along the thickness than the torsion or and unstressed samples. The strains exhibited in the tension sample seem to follow a similar trend to the torsion and unstressed sample. No large differences are observed between the three samples in either the radial or hoop

direction as shown in Figure 2.5b and 2.5c respectfully. In the hoop direction a large tensile strain is observed showing a large residual strain exists near the outer surface (Figure 2.5c). This is seen in the unstressed sample as well as both the deformed samples.

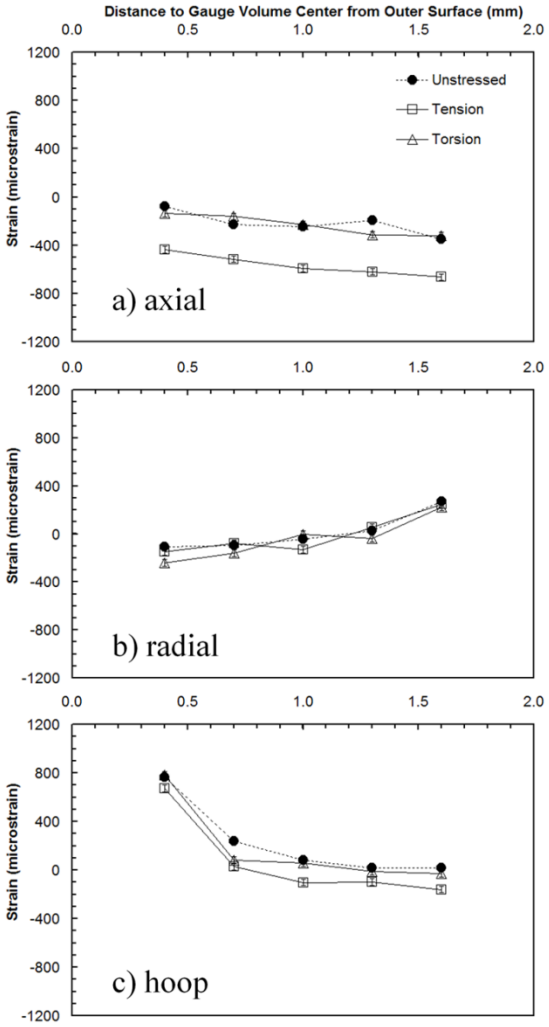

Figure 2.5 Residual strains in the Fe (110) plane for the (a) axial, (b) radial, and (c) hoop directions as a function of distance from the outer surface of the hollow cylinder, the error shown is two standard deviations of the strain.

The Fe (200) reflection shows the greatest differences in residual strains (Figure 2.6). For the axial direction, there are slightly higher tensile residual strains in the tension samples than in the other samples. In the radial (Figure 2.6b), the tension sample exhibits a tensile residual strain along the wall thickness greater than seen in the other samples. Unlike previous two cases, the radial direction does not seem to follow the same trend along the thickness as the unstressed and torsion samples. The hoop direction of the (200) reflection also shows a high shift in strain measured between samples. Also slightly compressive residual strains are observed in the torsion sample.

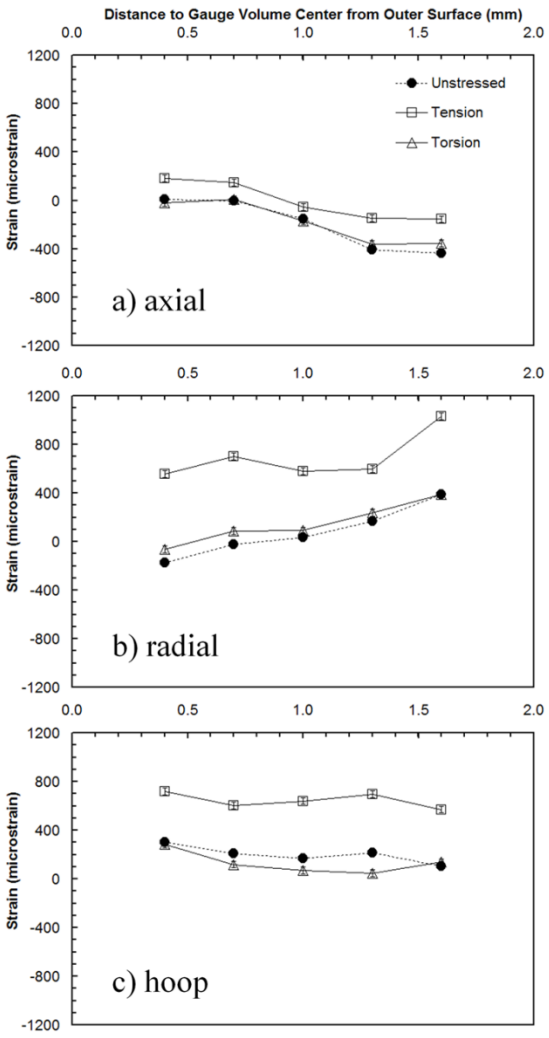

Figure 2.6 Residual strains in the Fe (200) plane for the (a) axial, (b) radial, and (c) hoop directions as a function of distance from the outer surface of the hollow cylinder, the error shown is two standard deviations of the strain.

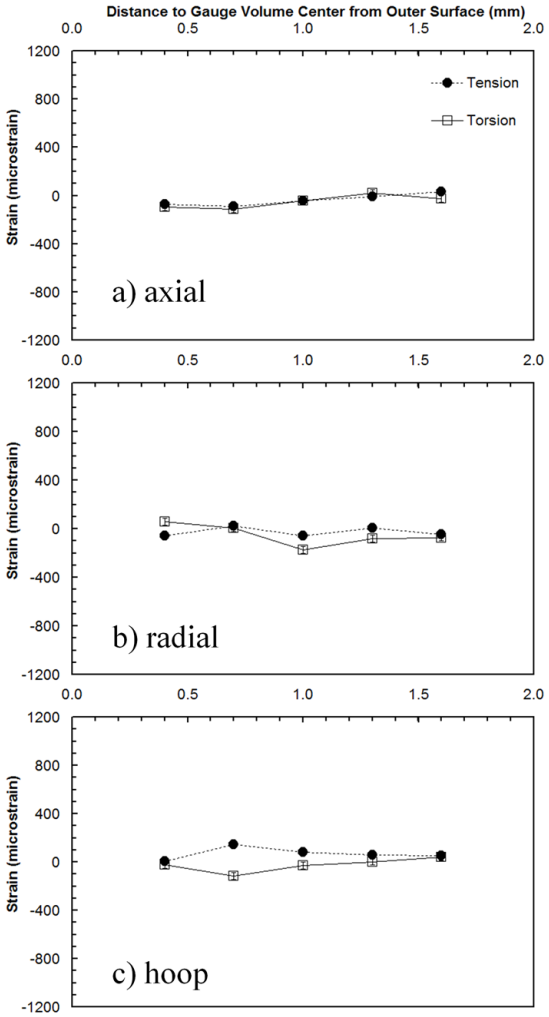

Figure 2.7 Normalized residual strains in the Fe (211) plane for the (a) axial, (b) radial, and (c) hoop directions as a function of distance from the outer surface of the hollow cylinder.

Initial State Approach

Figure 2.7 shows the normalized residual strain for the (211) reflection. No large values of residual strain were measured in any of the three directions measured for either deformed samples. Also, no large differences were observed between the data for the tension sample and the data from the torsion sample.

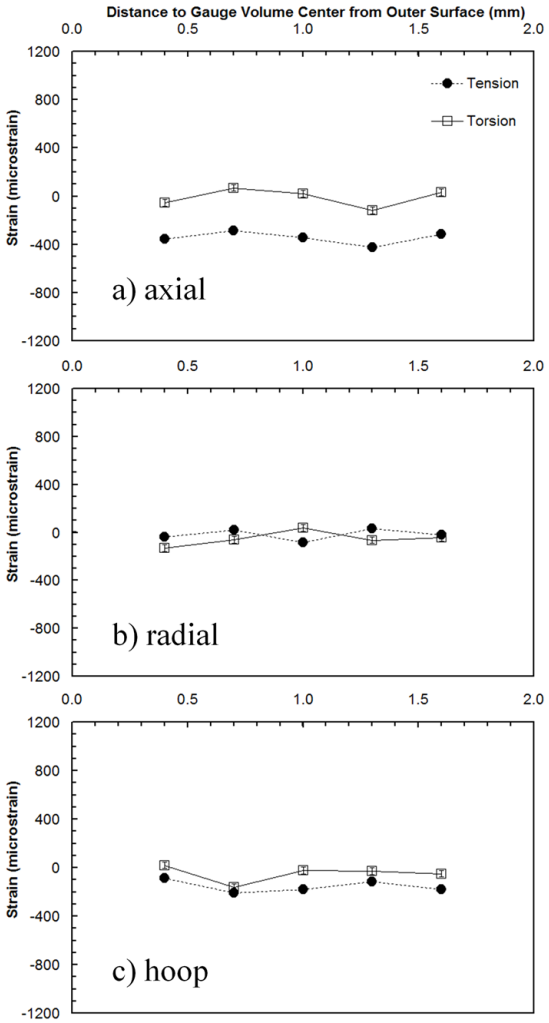

Figure 2.8 Normalized residual strains in the Fe (110) plane for the (a) axial, (b) radial, and (c) hoop directions as a function of distance from the outer surface of the hollow cylinder.

In the axial direction (Figure 2.8a) a large value of residual strain is observed. A compressive residual strain of 400 microstrain is seen in the sample subjected to axial deformation. Both the radial (Figure 2.8b) and hoop (Figure 2.8c) directions show no changes in residual strain beyond ±200 microstrain. In the hoop case the residual strains measured in the sample subjected to axial deformation tend to be tensile while the residual strains of the sample subjected to shear deformation seem to be more compressive.

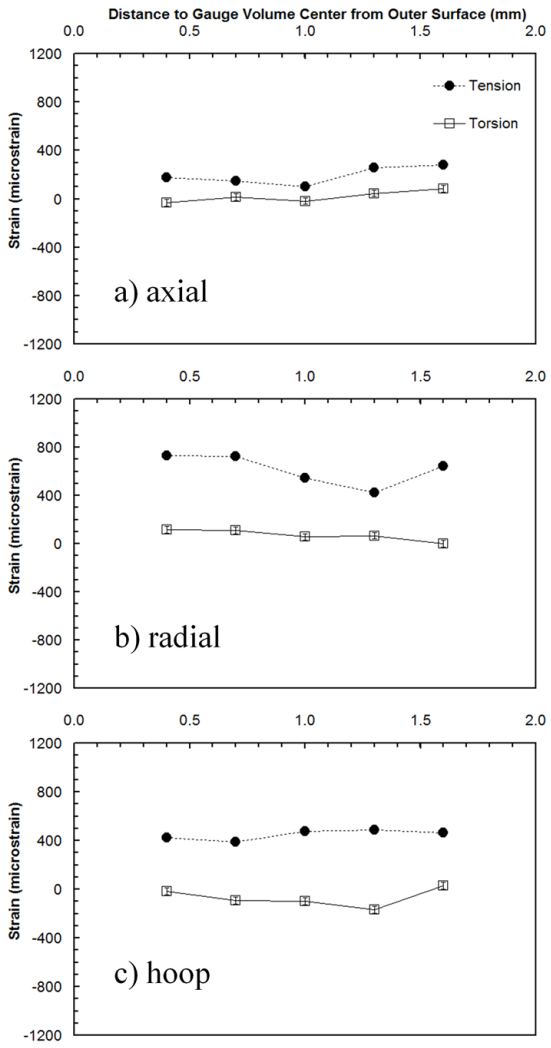

Figure 2.9 Normalized residual strains in the Fe (200) plane for the (a) axial, (b) radial, and (c) hoop directions as a function of distance from the outer surface of the hollow cylinder.

Figure 2.9 shows the normalized residual strain from the (200) reflection for each of the three directions. Changes in residual strain due to plastic deformation are seen in all directions. The least change in strain is seen in the axial direction (Figure 2.9a). The radial and the hoop directions in Figure 2.9b and 2.9b respectfully show large differences between samples. In all of the directions, the large values of residual strains measured for the sample subjected to axial deformation are tensile. All the samples subjected to pure shear deformation show little or no changes in residual strains in any of the directions.

Discussion and Summary

In this study, bcc steel alloy samples were subjected to pure torsion and pure tension to measure the residual strains for two *hkl* planes said to be insensitive to intergranular strains and one *hkl* plane that has been shown to be sensitive to intergranular strains. Considerable residual strains were observed in all samples. Gradients through thickness were observed in all samples. The trends observed through the wall thickness for the three samples were similar for all planes and strain directions measured. This similarity of trends between the unstressed sample and the deformed samples leads to the conclusion these trends are either an effect present in the sample due to their forming or due to constraints of a tubular shape on the deformations.

The results from the stress free approach show large gradients in residual strain across the cylinder wall thickness. In this approach d^0_{hkl} was determined from a powder sample. This is similar to how most residual strain studies are performed. The residual strain measured in this case is a convolution of both the strains formed by the manufacture of the tubular samples as well as the residual strains induced by the applied plastic deformations.

It is important to note that one determination is that the large gradients observed in the stress free approach are not observed in the initial state approach. This means that these large gradients must be an effect of the sample manufacturing process. By using the initial state approach the effect of the plastic deformation can be successfully de-convoluted form the manufacturing process. This is an important consideration when choosing an adequate d^0_{hkl} for experiments.

The results from the initial state approach were most revealing. As expected, the Fe (211) reflection shows the least difference in the residual strain measured in the tension sample in all

directions. This shows that this plane is insensitive to effects of intergranular strains as Hutchings' states (Hutchings et al., 2005).

The Fe (110) axial case shows much greater values of residual strain due to axial deformation than expected from Hutchings. The (110) plane is stated to be insensitive to the effects of intergranular strains. If this was the case, then data similar to the (211) plane is expected. However, strains measured in the axial direction of the (110) reflection yielded higher values of measured residual strain due to axial deformation than that of the axial direction of the plane expected to be the most sensitive, the (200). The radial and hoop directions of the (200) reflections do show the greatest changes in residual strains in each of their respective directions. This was expected from Hutching statement (Hutchings et al., 2005).

Little differences were seen in the measured residual strain data for the sample subjected to shear deformation in the reflections measured. Residual strains measured in the torsion sample did differ greatly from that of the tensile sample.

Although this study has shown the sensitivity of the measured planes to axial deformation, none of the planes measured in this study are sensitive to the application of pure shear deformation.

To conclude, the study has sufficiently shown that residual strains' sensitivity to plastic deformation depends on the mode of deformation. It is clear that two different modes of plastic deformation that generate the same octahedral shear strain invariant do not necessarily generate similar sensitivity in residual strain measurements. Further study could be conducted by measuring residual strains in samples that have been subjected to shear strains greater than those in this study. A much more effective manner of performing the said experiment strains would be to perform an in-situ torsional study.

CHAPTER 3. RESIDUAL STRAIN EVOLUTION: GENERALIZED LEAST SQUARED METHOD

Abstract

Evaluating the state of residual strain or stress is critically important for structural materials and for reliable design of complex shape components that need to function in extreme environments subjected to large thermo-mechanical loading. When the residual stress state is superimposed with external loads, reduction or increase in yield strength can occur. Past diffraction studies for evaluating the residual strain state involved measuring lattice spacings in three orthogonal directions, which often do not correspond to principal directions. To completely resolve the state of strain at a given location, a full strain tensor must be determined. This is especially important when characterizing materials exposed to biaxial or complex loading. Neutron diffraction at the 2nd Generation Neutron Residual Stress Facility (NRSF2) at Oak Ridge National Laboratory is used in this study to measure strain tensors associated generated from the application the of varied stress paths. Hollow cylinder steel samples with a two a mm wall thickness are subjected to either pure axial extension or pure torsion. A virgin sample that is not subjected to any additional deformation, but is produced with identical manufacturing conditions and machining steps involved to obtain hollow cylinder geometry provides reference d-spacings for given hkl planes at targeted spatial location(s). The two samples which are subjected to either pure tension or torsion are loaded to a deformation state that corresponded to equal amount of octahedral shear strain which is an invariant. This procedure is used so that a basis for comparison between the two samples can be made to isolate the stress path effects. A 2-circle Huber orienter is used to obtain strain measurements on identical gauge volume at a series of ϕ and ψ values. The residual stress tensor corresponding to *ex situ* (upon unloading) conditions are presented for three lattice planes (211, 110, 200) for a bcc ferretic system exposed to tension and pure torsion.

Introduction

An understanding of the state of the residual strain tensor resulting from exposure to complex thermo-mechanical loading history provides essential information to evaluate the service limits of a given metallic component. Neutron diffraction is a well-established technique for measuring residual strains within the bulk of engineering materials (Allen et al., 1985; Hutchings et al., 2005; I.C. Noyan & Cohen, 1987; J. W. L. Pang et al., 1998; Withers et al., 2007). Neutrons are unique in their ability to probe non-destructively at depth within large as-machined parts to measure sub-surface strains. In contrast, typical laboratory x-ray techniques are widely used for measurement at or near the surface of a sample (I.C. Noyan & Cohen, 1987).

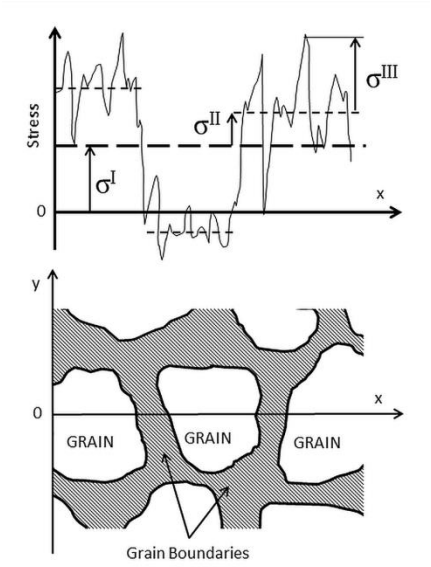

Figure 3.1 Visualization of type I, II, and III stresses in a polycrystalline material

Depending on the scale of the measurement region in a polycrystalline material, residual stresses may be divided into one of three categories: type I (σ^{I}), type II(σ^{II}), or type III(σ^{III}) stresses (Hutchings et al., 2005). Shown graphically in Figure 3.1, type I stresses, also referred to as macrostresses, extend across many grains in a sample, and their length scales are on the order

of millimeters. Type I stresses are assumed to be continuous across grains and across phase boundaries. Type II stresses act in a region comparable to the grain size of the polycrystalline material and is discontinuous from grain to grain. The length scale associated with type II stresses is on the order of tens of microns. Type III stresses are stresses that vary within a single grain across crystal defects, dislocations, or vacancies. Both type II and type III stresses are referred to as microstresses.

In this study, the stresses measured through neutron diffraction correspond with the shift of a Bragg peak and are considered to be continuous across the measured gauge volume. The gauge volume used contains many grains. Therefofre in this study the residual stress measured is best classified as a σ^{I} stress.

Much of the current literature on residual stress and strain evolution as a function of applied loading history is performed using uniaxial loading, largely using tensile testing (Clausen et al., 1999; J. W. L. Pang et al., 1998). However, many engineering components are subjected to complex multi-axial loading, and shear stress dominates yield (Yu, 2002).

To fully describe the response of a material exposed to a complex state of loading, a rank-2 symmetric strain tensor needs to be determined to completely describe the six independent quantities associated with three normal and three shear strains. From the measured tensor, one can deduce the major, intermediate, and minor principal strain amplitudes ϵ_1, ϵ_2, ϵ_3 respectively and their corresponding directions (Dieter, 1986; Eringen, 1980; Malvern, 1969; Mase, 1970).

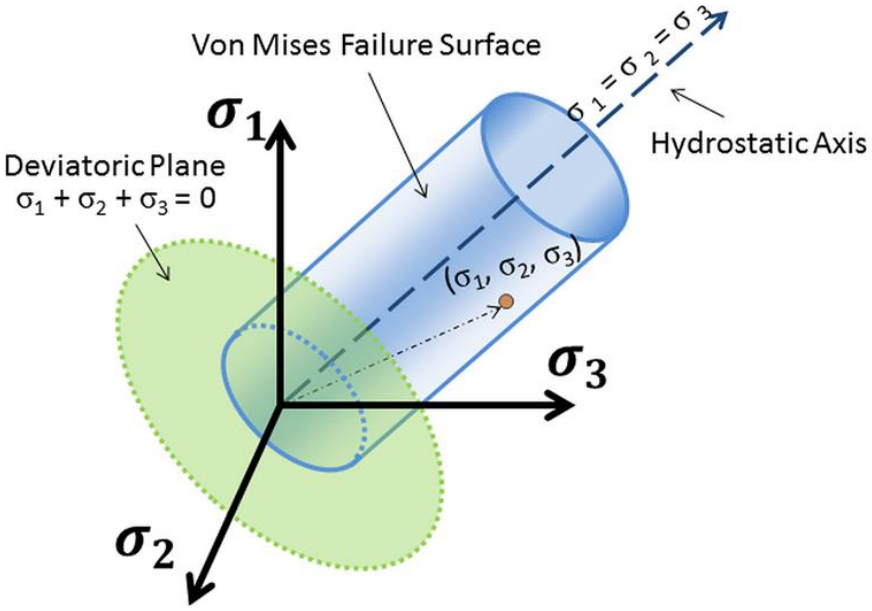

Figure 3.2 Graphic describing Height-Westergaard space (stress space). Shown within the figure is a given point defined by principal strains (ϵ_1, ϵ_2, ϵ_3), the von Mises yield surface (blue cylinder) and the deviatoric plane (green).

Octahedral shear strain is an important invariant often considered in describing the deformation behavior of solids. This invariant also serves as a basis for comparison of differences in behavior resulting from various applied stress paths. The octahedral shear strain is defined as

$$\gamma_{oct} = \frac{2}{3}\sqrt{(\epsilon_1 - \epsilon_2)^2 + (\epsilon_2 - \epsilon_3)^2 + (\epsilon_3 - \epsilon_1)^2} \qquad (3.1a)$$

this corresponds to:

$$\gamma_{oct} = \frac{2}{3}\sqrt{(\epsilon_{11} - \epsilon_{22})^2 + (\epsilon_{22} - \epsilon_{33})^2 + (\epsilon_{33} - \epsilon_{11})^2 + 6(\epsilon_{12}{}^2 + \epsilon_{23}{}^2 + \epsilon_{13}{}^2)} \qquad (3.1b)$$

for the strain tensor shown below:

$$\varepsilon_{ij} = \begin{bmatrix} \epsilon_{11} & \epsilon_{12} & \epsilon_{13} \\ \epsilon_{21} & \epsilon_{22} & \epsilon_{23} \\ \epsilon_{31} & \epsilon_{32} & \epsilon_{33} \end{bmatrix} \quad (3.2)$$

Strain and stress tensors are most effectively visualized in three dimensions as shown in Figure 3.2. Figure 3.2 also shows another invariant, the von Mises stress that is often used in defining yield behavior of polycrystalline metals with little or no texture.

While extensive studies of residual strain resulting from the application of uniaxial state of stress (tensile or compressive) have been performed, a very limited number of studies have been carried out to investigate three dimensional residual stress/strain tensors due to the complex nature of residual stress (Brown et al., 2003; Larsson, Clausen, Holden, & Bourke, 2004; J. Pang et al., 2000; Shute, Cohen, & Jeannotte, 1988). Winholtz et al. previously explored complex states of strain and their evolution during heat treatment for a specific weld (R. Winholtz & Krawitz, 1995). In the case of the welds studied, the stress path is not readily defined as the state of stress arises from complicated interactions between temperature, stress, strain, and phase transformations.

This current study seeks to evaluate the complex state of residual strain tensors resulting in a steel alloy that has been subjected to controlled stress paths that yield an identical octahedral shear strain value achieved through either pure tensile or torsional loading.

For cylindrical samples, residual strain measurements using neutron diffraction often involve orienting the beam and detector configuration such that the resulting scattering vector provides information on three orthogonal strain vectors in the axial, radial, and circumferential direction. For uniaxial loading within the elastic limit these three directions are the principal strain directions. However, for cases of complex loading these measured normal strains typically

co-exist with shear strain. The shear strains typically are not captured in the three orthogonal measurements along the radial, circumferential, and axial directions, and thus the measured strains are not necessarily principal strains (J. Bunn, Penumadu, & Hubbard, 2010; Davydov, Lukas, Strunz, & Kuzel, 2009; Hutchings et al., 2005).

Frequently in engineering materials, the average strain (macro strain) is measured using surface mounted strain gauges, surface digital image correlation techniques, or extensometers. These strains are considered to represent an average response of the material to applied or residual stress. In comparison, *hkl* specific lattice strain responses can vary depending on the lattice planes investigated, and these variations result from anisotropy of single crystals represented by the grains in the polycrystalline metals.

Previous studies on the evolution of lattice specific residual stress/strain to the application of uniaxial tension were performed to determine material behavior (Clausen et al., 1999; J. W. L. Pang et al., 1998). For instance, the lattice specific Young's modulus (E_{hkl}) for the (211) plane in a steel (bcc) is expected to be approximately 200GPa-230GPa while the E_{hkl} for the (200) plane is much softer in the range of 125Gpa – 175Gpa.

For measurement of the macro shear strain response, typically surface mounted strain rosettes or surface digital image correlation techniques are used. A strain rosette is a collection of three uniaxial strain gauges arranged in a pre-determined geometric configuration. One strain gauge measures along the axial direction of the sample, and the two additional strain gauges measure at a target inclination, for example at ±45°. If one considers the surface of a deforming cylinder, a plane strain condition can be assumed and the following relate the strain measured by three unidirectional strain gauges along a, b, and c axis:

$$\begin{cases} \varepsilon_a = \dfrac{\varepsilon_\theta + \varepsilon_z}{2} + \dfrac{\varepsilon_\theta - \varepsilon_z}{2} cos2\alpha + \varepsilon_{r\theta} sin2\alpha \\ \varepsilon_b = \dfrac{\varepsilon_\theta + \varepsilon_z}{2} + \dfrac{\varepsilon_\theta - \varepsilon_z}{2} cos2(\alpha+\beta) + \varepsilon_{r\theta} sin2(\alpha+\beta) \\ \varepsilon_c = \dfrac{\varepsilon_\theta + \varepsilon_z}{2} + \dfrac{\varepsilon_\theta - \varepsilon_z}{2} cos2(\alpha+\beta+\gamma) + \varepsilon_{r\theta} sin2(\alpha+\beta+\gamma) \end{cases} \quad (3.3)$$

The directly measured strain from the rosette can then be used to solve for the strain tensor on the surface (ϵ_r, ϵ_θ, and $\epsilon_{r\theta}$). The engineering shear strain, $\gamma_{r\theta}$ is as follows:

$$\gamma_{r\theta} = \varepsilon_{r\theta} + \varepsilon_{\theta r} = 2\varepsilon_{r\theta} \quad (3.4)$$

A challenge encountered in attempting to investigate the microstructural *hkl* dependent response to pure shear strain using neutron diffraction is that only the normal strain (strain perpendicular to the given *hkl* lattice planes) can be directly deduced from the diffraction measurements. This is because d-spacing measurements only determine deformations between the lattice planes. However, shear strains behave fundamentally different than normal strains so a more robust measurement scheme is required to measure the response of a polycrystalline sample to applied shear(Bickford, 1998; Meyers & Chawla, 1984; Timoshenko, 1962) using neutron diffraction technique.

The measurement of the residual (after unloading) strain state using the typical methodology of mapping three geometrically orthogonal strain vectors has been reported previously for materials exposed to pure tension and pure torsion (J. Bunn et al., 2010). This early study on isolating the impact on the deformation behavior on residual strain corresponding to pure torsion was obtained for three orthogonal directions (axial, radial and hoop). This study concluded that no residual strain was measured along the radial, hoop, and axial directions even

though the samples were subjected to large plastic strains through pure torsion. Based on this conclusion, the authors hypothesized that residual strains may exist in orientations that did not correspond to the three orthogonal directions considered in the measurement. This effect is due to plane sections remaining plane and out-of-plane warp being minimal with a radially symmetric cross section, which is employed for the sample geometry studied. One would also expect a maximum normal strain of a cylindrical sample subjected to simple shear should be at 45° inclined from the axial direction.

The need for a general method to determine the strain tensor using diffraction has been addressed previously. Winholtz and Cohen proposed a method using a least squared fitting to determine the strain tensor from multiple orientations of the scattering vector for an identical spot size and/or gauge volume (approximately same sub-set of grains participating in diffraction) (R. A. Winholtz & Cohen, 1988). The basis for this technique can be found in the work of Noyan (I.C. Noyan & Cohen, 1987) and that of Nye (Nye, 1985). This technique was applied in this study and is described in the experimental section in detail.

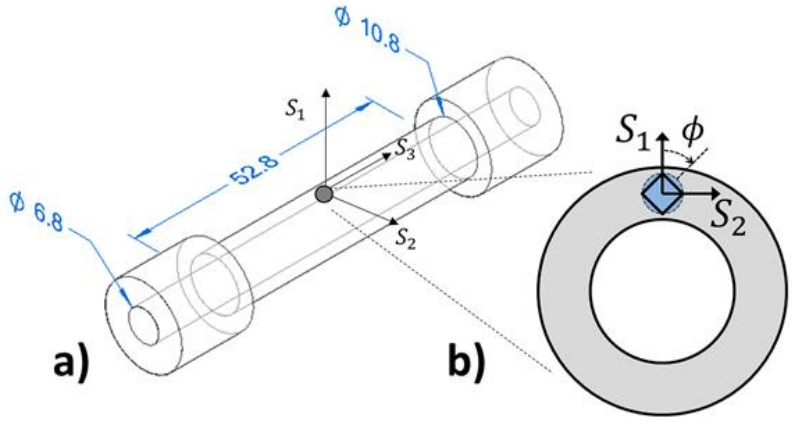

Figure 3.3a) Sample dimensions for the hollow cylinder used in the experiments and b) gauge volume location and effective gauge volume (approximately spherical) over all combinations of ϕ and ψ

Samples

Hollow cylindrical samples, as shown in in Figure 3.3, were used in the experiments. The samples were machined from 12L14 alloy steel. The material was a single phase bcc ferretic steel alloy, and it was expected that some inclusions may exist from precipitates at the grain boundaries. Three initially (prior to applying either tensile or torsional deformation) identical samples were used in the study. One sample (tensile) was subjected to axial deformation using a combined axial-torsional servo-hydraulic loading system that was PID controlled ensuring that no torsional shear stress was applied to the sample. Another sample (corresponding to the applied state of torsion) was subjected to pure shear loading using the same load frame with PID control targeting zero axial stress. The third sample (reference) was not deformed. Both samples that were subjected to either tensile or torsional loading were deformed well beyond yield to a target value of octahedral shear strain invariant plastic strain. The average shear strain in a hollow cylinder ($\gamma_{\theta z}$) was given by the equation,

$$\epsilon_{\theta z} = \frac{2\theta({r_o}^3 - {r_i}^3)}{3h({r_o}^2 - {r_i}^2)} \tag{3.5}$$

where r_0 and r_i are the outer and inner radii of the cylinder respectively. The angle of twist was given by ω, and h describes the gauge height of the sample. The reference sample, not subjected to any deformation post machining was used for an accurate determination of initial lattice spacing of the as formed state of the alloy prior to deformation, considered to be a the reference state. Figure 3.4a and Figure 3.4b show the global true stress-strain history applied to the sample using tensile and torsional modes respectively. The strain was measured using a surface mounted

strain gauge stacked rosette at the center of the gauge length of the deforming hollow cylinder samples.

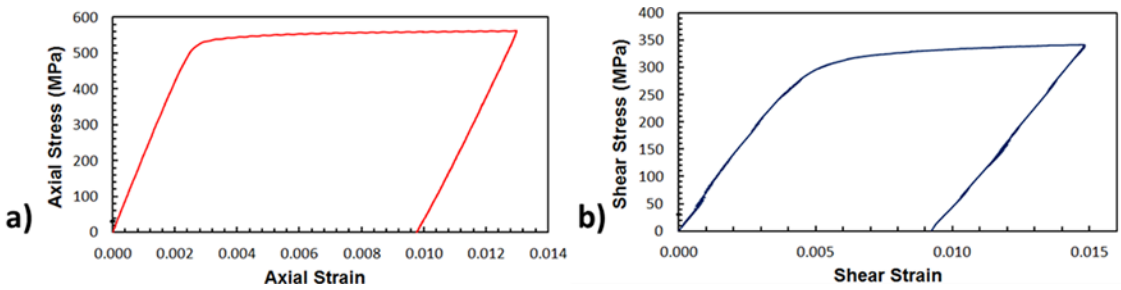

Figure 3.4 Macro stress-strain history for hollow cylinder subjected to a) uniaxial tension through axial deformation or b) simple shear through application of torsion

Each of the samples were deformed plastically to the same amount of octahedral shear strain (Equation 3.5) before unloading. Figure 3.5 compares deformation histories of the deformed samples in terms of octahedral shear stress versus octahedral shear strain, each being invariants. Both samples were subjected to a maximum value of γ_{oct} of approximately 1.2%prior to unloading. It is important to notice that this value of octahedral shear strain was achieved through different paths, one case by uniaxial tension through application of axial strain of 0.0130 and in the other case through torsional shear applying a shear strain of 0.0150. By subjecting both samples to an identical maximum value of strain invariant, it was then possible to isolate the effects of residual strain evolution at the end of unloading with the stress path (tension versus torsion) corresponding to different loading/deformation history.

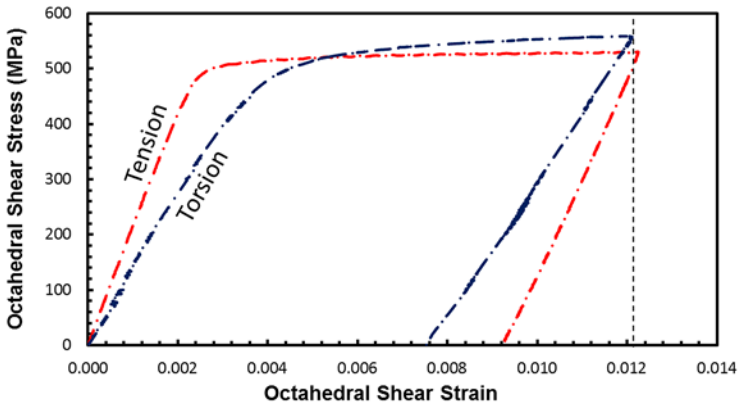

Figure 3.5 Macro octahedral shear stress versus octahedral shear strain history for the two samples subjected to different load paths

Neutron Strain Mapping Experimental Setup

The neutron experiments for evaluating lattice strain measurements on ex-situ samples subjected to multi-axial loading were performed at the 2nd Generation Neutron Residual Stress Mapping Facility (NRSF2) at the High Flux Isotope Reactor (HFIR) at ORNL. The details of the instrument are provided elsewhere(Oak Ridge National Laboratory, 2009). Essential features required to carry out the planned experiments were available at HFIR-NRSF2 instrument with the availability of high flux, ability to use small gauge volumes (0.5 mm^3) to obtain diffraction data with acceptable signal to noise ratio, and accurate sample alignment (positioning within 100 microns of target gauge volume location) through the use of laser based tracking system integrated with SScanSS software (Cornwell, Bunn, Schmidlin, & Hubbard, 2012; J. A. James et al., 2008; J. A. James et al., 2004).

Lattice specific strains in the bulk material were obtained using neutron diffraction by measuring the *hkl* specific atomic planar spacings (d-spacings) for a chosen volume location

within the wall thickness of the deformed and virgin steel tubes. The technique has been described in detail previously.

In this study, measurements for the (211), (110) and (200) *hkl* lattice planes were obtained. Previous experiments by the authors and past literature indicates that the (211) plane is the most pertinent plane to consider when one is interested in obtaining lattice strain behavior to closely represent the engineering strain measured by an extensometer or a strain gauge mounted on a deforming specimen(Hutchings et al., 2005; R. Woracek, J. R. Bunn, D. Penumadu, & C. R. Hubbard, 2012). Previous experiments also showed that the (110) and (200) planes are both sensitive to intergranular strains induced by plastic deformation.

The diffraction strain measurements are relative to a measured value of a stress-free sample. In this study, an undeformed reference cylinder (as machined) was used for obtaining the reference d_0 lattice spacing corresponding to a target gauge volume location through the wall thickness of a cylindrical specimen that was subjected to target shear or axial strain. Using a reference cylindrical steel alloy specimen that has experienced a similar history of processing during its manufacturing eliminates the possibility of effects of formation and machining by considering their effect in initial planar spacing prior to the application of tensile/torsional deformation. This ensures that only the residual strains resulting from the plastic deformation history after unloading from a target octahedral; strain value (as shown in Figs. 4a, 4b and 5) are measured.

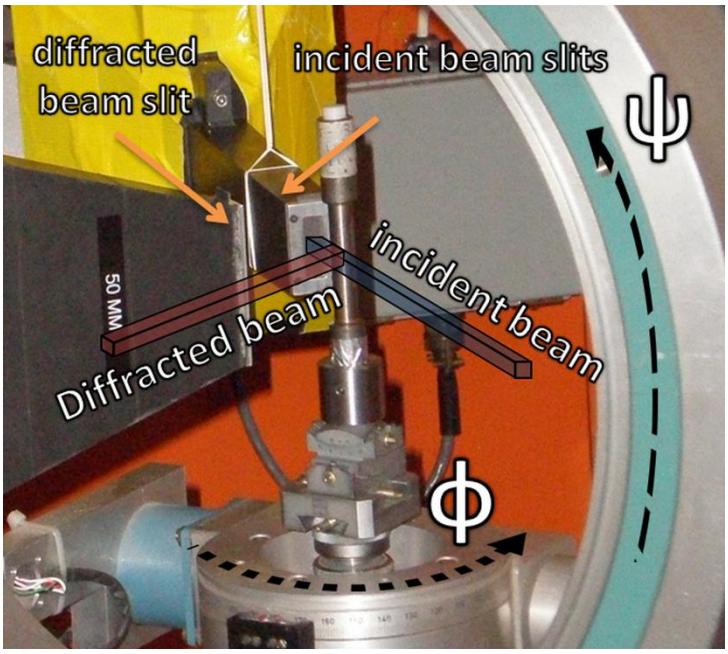

Figure 3.6 Setup showing the sample on the 2-circle orienter mounted on the NRSF2 goniometer with definition of the rotation axes ϕ and ψ. The ψ plane bisects the incident and diffracted beam

In the technique proposed by Winholtz and Cohen, (R. A. Winholtz & Cohen, 1988) a minimum of six independent components of the strain tensor must be measured for the same gauge volume using rotations of the sample about the center of the gauge volume. In this study a Huber 2-Circle orienteer was mounted on the NRSF2's XY table as shown in Figure 3.6. The angle ψ corresponds to the horizontal (X) axis of the instrument, and the angle ϕ about the vertical (Z) axis of the instrument at ψ = 0. Figure 3.6 shows the cylindrical sample mounted on the Huber orienteer and corresponding rotations. Figure 3.6 shows the incident and diffracted beams as well as the ϕ and ψ rotations in relation to the instrument coordinate system. The neutron diffraction based d-spacing measurements for the various ϕ and ψ rotations were used to solve for the strain tensor ϵ_{ij} using Equation 3.6 proposed by Noyan and Cohen (I.C. Noyan & Cohen, 1987) for a polycrystalline material and previously by Nye (Nye, 1985):

$$\epsilon_{\phi\psi} = \epsilon_{11}\cos^2\phi\sin^2\psi + \epsilon_{22}\sin^2\phi\sin^2\psi + \epsilon_{33}\cos^2\psi + \epsilon_{12}\sin 2\phi\sin^2\psi + \epsilon_{13}\cos 2\phi\sin 2\psi + \epsilon_{23}\sin\phi\sin 2\psi, \quad (3.6)$$

The sample and instrument coordinate systems are shown in Figure 3.7 and angles between the sample axes and laboratory axes are defined. At least six combinations of ϕ and ψ are required for the measurement of a complete strain tensor (Nye, 1985). In practice, more than six combinations of ϕ and ψ should be used for improved statistics based on implementing least squares data reduction technique. During the experiment, a sample was mounted and aligned on the Huber orienteer such that for any set of ϕ and ψ values corresponding to a given diffraction pattern the gauge volume location does not change. The measurement procedure described above was then implemented for all the three specimens. A complete strain tensor for three separate *hkl* planes were mapped using 30 independent sets of ϕ and ψ, rotations for a chosen gauge volume. The reference sample was measured only at target gauge volume centroid locations using nine combinations due to a lack of availability of instrument time.

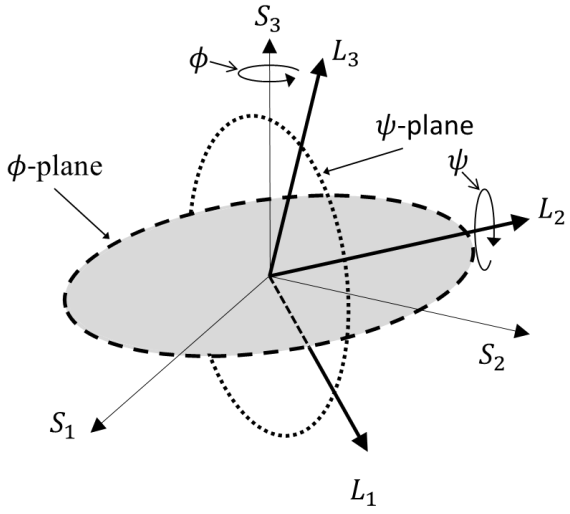

Figure 3.7 Relationship between the laboratory (L) and the sample coordinate systems (S)

Strains were measured using a gauge volume of $1x1x1mm^3$ defined by the incident and diffracted beam slits with the gauge volume centered at the midpoint between the inner and outer diameter of the sample cylinder. The gauge volume used was symmetric such that under the various combinations of ϕ and ψ a similar averaging over the gauge volume was achieved in each measurement. The small gauge volume also assures that the gauge volume was fully within the wall for any rotation of the specimen. This prevented any artificial shifts of the measured d-spacing due to partial filling of the gauge volume (Wang et al., 1998) with air.

Due to the radial dependence of shear stress in a cylindrical sample, a careful and precise alignment procedure was proven very crucial in order to assure that the same gauge volume location was defined for each measurement. A positioning accuracy of the gauge volume location smaller than 0.10 mm was required to achieve an uncertainty of 5% in the calculated shear stress. This accuracy was reached by using a laser alignment system, consisting of a FARO laser tracker and SScanSS software developed at Open University(James JA, 2008) to align the sample to as little as 0.05 mm error in gauge volume centroid placement.

Experimental Results

The (110) and the (200) planes had significant differences in measured residual strain tensors based on whether the steel specimen was subjected to deformation through uniaxial tension or through simple shear through pure torsion The dependence on load path was much more pronounced in the cases of the (110) and the (200) planes. The interpreted principal strains and stresses from neutron diffraction are listed in Table 3.2. The largest values of residual strain were observed for the (211) plane. The magnitude of residual strain generated in the (110) and the (200) plane were an order of magnitude lower than those obtained for the (211). Considering

all the measurements, the (200) plane shows the largest differences between the two load paths. This was evident in the reported principal strain and stress response of the (200) plane.

Table 3.1 Measured lattice specific strain tensors from the least squared fitting of collected data for each load path studied.

Tension [micro-strain]	**Torsion [micro-strain]**
$\boldsymbol{\varepsilon_{211}} = \begin{bmatrix} \mathbf{1562} & \mathbf{-462} & \mathbf{838} \\ \mathbf{-462} & \mathbf{-29} & \mathbf{-122} \\ \mathbf{838} & \mathbf{-122} & \mathbf{-8} \end{bmatrix}$	$\boldsymbol{\varepsilon_{211}} = \begin{bmatrix} \mathbf{2040} & \mathbf{-571} & \mathbf{915} \\ \mathbf{-571} & \mathbf{141} & \mathbf{-74} \\ \mathbf{915} & \mathbf{-74} & \mathbf{-8} \end{bmatrix}$
$\boldsymbol{\varepsilon_{110}} = \begin{bmatrix} \mathbf{-277} & \mathbf{-135} & \mathbf{102} \\ \mathbf{-135} & \mathbf{-252} & \mathbf{12} \\ \mathbf{102} & \mathbf{12} & \mathbf{218} \end{bmatrix}$	$\boldsymbol{\varepsilon_{110}} = \begin{bmatrix} \mathbf{5} & \mathbf{-223} & \mathbf{259} \\ \mathbf{-223} & \mathbf{-161} & \mathbf{110} \\ \mathbf{259} & \mathbf{110} & \mathbf{63} \end{bmatrix}$
$\boldsymbol{\varepsilon_{200}} = \begin{bmatrix} \mathbf{-333} & \mathbf{-440} & \mathbf{14} \\ \mathbf{-440} & \mathbf{-29} & \mathbf{252} \\ \mathbf{14} & \mathbf{252} & \mathbf{102} \end{bmatrix}$	$\boldsymbol{\varepsilon_{200}} = \begin{bmatrix} \mathbf{32} & \mathbf{-422} & \mathbf{-3} \\ \mathbf{-422} & \mathbf{145} & \mathbf{285} \\ \mathbf{-3} & \mathbf{252} & \mathbf{-53} \end{bmatrix}$

Because principal stresses calculated from the stress tensor occur in three dimensions it is important to quantify the transformation between the as-received samples (with no post formation stresses) and each of the samples subjected to plastic deformation. The angles ω_1, ω_2, and ω_3 correspond to the angles between the axes of the maximum, intermediate and minimum stresses of the as-received sample and the axes of the maximum, intermediate and minimum principal stresses of the deformed sample, respectively. To clarify, the angle ω_1 would correspond to the rotation of the maximum principal residual stress vector for the deformed sample from the maximum residual stress vector for the as-received sample. The angles ω_1, ω_2, and ω_3 are repoted for each of the loading cases and for each hkl in Table 3.3.

Table 3.2 Calculated principal strains and corresponding principal stress values for axial versus torsional loading. Strain values reported in microstrains. E_{hkl} data (utilized from previous study) is also shown for conversion from residual strain to stress.

	***hkl* = (211)**				***hkl* = (110)**				***hkl* = (200)**			
	Tension		**Torsion**		**Tension**		**Torsion**		**Tension**		**Torsion**	
	Strain [μstrain]	**Stress [MPa]**	**Strain [μstrain]**	**Stress [MPa]**	**Strain [μstrain]**	**Stress [MPa]**	**Strain [μstrain]**	**Stress [MPa]**	**Strain [μstrain]**	**Stress [MPa]**	**Strain [μstrain]**	**Stress [MPa]**
Maximum	2033	480	2539	639	239	9	313	41	262	-15	591	76
Intermediate	-118	127	77	236	-138	-50	39	-1	-58	-51	-28	5
Minimum	-390	83	-293	175	-411	-92	-434	-75	-866	-144	-440	-42
Elastic constants used (R. Woracek et al., 2012)	**E_{hkl} = 208 GPa, G_{hkl} = 103 GPa, υ = 0.27**				**E_{hkl} = 197 GPa, G_{hkl} = 90 GPa, υ = 0.27**				**E_{hkl} = 146 GPa, G_{hkl} = 50 GPa, υ = 0.27**			

Table 3.3 Calculated principal stress rotations (ω_1, ω_2, and ω_3) between the as-received sample principal axes and the deformed samples principal axes.

	ω_1 [deg.]		**ω_2 [deg.]**		**ω_3 [deg.]**	
hkl	**Tension**	**Torsion**	**Tension**	**Torsion**	**Tension**	**Torsion**
211	26.2	21.8	102.9	103.1	67.6	69.3
110	78.4	136.1	91.8	79.4	11.8	131.9
200	111.2	124.7	59.1	41.3	38.9	70.4

As seen in Table 3.3, the rotations of the principal strain axes vary the greatest in the case of the 110 plane and are most similar in the 211 plane. The largest difference in rotation is that of ω_3 in the 110 plane.

The calculated octahedral shear stress invariants for each load case are shown in Table IV. In both Table 3.2 and Table 3.4, authors used suitable values for E_{hkl} and G_{hkl} from a previous study for the identical alloy and sample deformation modes(R. Woracek et al., 2012). The octahedral shear stress invariants presented in Table 3.4 (calculated from Equation 3.1a) show that in the (211) and (200) planes, the torsion case resulted in a greater value of the octahedral residual shear stress invariant.

A direct comparison of the residual octahedral shear strain γ_{oct} of the sample subjected to tensile deformation versus pure torsional deformation shows a 16% increase in residual octahedral shear strain in both the (211) and (110) planes when the sample was subjected to torsion. However, the (200) residual octahedral shear strain is unchanged regardless of the applied load path. The small change of 5MPa observed in the (200) sample is within the expected error of the analysis.

Table 3.4 Calculated principal stresses and octahedral shear stress invariants for both load paths explored. Data for hkl specific shear moduli from previous study.

hkl	**Shear Modulus, G_{hkl} (GPa) (R. Woracek et al., 2012)**	**Residual Octahedral Shear Stress Invariant (MPa)**	
		Tension	**Torsion**
211	103	223.3	259.0
110	90	48.0	55.5
200	50	47.5	42.4

Discussion and Conclusions

Results from the study show that residual strain tensors generated by differing stress paths can result in a state of residual stress that is substantially different from uniaxial tension case. This study demonstrates that such differences can only be ascertained by evaluating a full residual strain/stress tensor using Huber circle approach as presented here for ex-situ samples. The lattice specific strain tensors shown in Table 3.1 differ greatly upon examination of measured results.

However it is important to realize that differing strains will exist for the tensor components upon rotation of the rank-2 tensor. Therefore, it is essential to compare the principal strains calculated from the measured tensors and to compare the lattice specific octahedral shear strains representing an invariant quantity for readily comparing loading path differences.

The experiments have shown that a full residual strain tensor response in bulk polycrystalline materials is measurable with significant precision using small gauge volumes (for both uniaxial tensile deformation as well as torsional loading). The exploration of lattice specific residual strain tensors demonstrates that different material planes in the bcc system respond differently to the same applied octahedral shear strain achieved through two independent load paths. Of the planes explored, the (211) and (110) planes demonstrate a dependence on applied load path. However, the (200) plane does not The results demonstrate the need for implementing multi-axial loading conditions integrated with neutron diffraction based strain mapping techniques.

Present work also demonstrates that simply measuring residual strains in three orthogonal directions (axial, radial, and hoop, in the case of a cylindrical sample), which is often convenient

to implement at neutron instruments, is not sufficient to describe the complete response of a polycrystalline material to complex or biaxial loads as the loading will undoubtedly rotate the generated residual strain increments away from the three orthogonal directions corresponding to a plate or a cylindrical geometry. Furthermore, understanding the full state of strain that exists in a sample, including the ability to calculate principal strains and strain invariants directly from this measured data, will help residual strain measurements better explore and quantify the effects of complex and biaxial loadings on engineering materials. Additionally information about the rotation of the principal strains can be utilized in the minimization of corrosion and fatigue cracking location. Without the rotation and principal stress information cracking could be induced in rotations other than those explored in traditional means through complex loading, Although time consuming, mapping measurements can be performed with precise alignment using a laser tracker combined with the SScanSS software. These diffraction results can then be utilized in conjunction with FEM model results for understanding three dimensional deformation behavior and residual stress evolution.

With the technique presented in this paper lattice specific residual strain states can be measured reliably as long as the count times for that specific *hkl* and the grain size of the material is reasonably small in comparison to the measured gauge volume. The most practical application of full tensor measurement may exist in the case of high penalty of yield parts with complex geometry, loading histories, chemistry and phase changes and/or temperature effects, such as nuclear reactor and aerospace components. In these cases, the full strain response in a polycrystalline material on an *hkl* lattice response will be even more difficult to predict and much more impactful for implementing more reliable design practices.

CHAPTER 4. METHOD TO DETERMINE HKL STRAINS AND SHEAR MODULI UNDER TORSION USING NEUTRON DIFFRACTION

Abstract

An experimental method, using *in-situ* neutron diffraction for the measurement of shear strain, based on (*hkl)* lattice spacing changes under torsional loading, is described. This method provides the ability to probe the response of crystallographic planes to application of shear stress, inside the bulk of samples that are subjected to torsion. To demonstrate the method, shear moduli corresponding to bcc (211), (200) and (110) were experimentally determined for a solid cylinder of ferritic alloy 12L14 under elastic loading. Results indicate that the elastic constants determined under torsional shear show a different degree of anisotropy than those obtained from tensile loading.

Introduction

The lattice strain response of polycrystalline materials under deformation is usually characteristic for each lattice plane family *hkl*, because the stiffness of a crystal is generally anisotropic.(Chung & Buessem, 1967; Hutchings et al., 2005) In polycrystalline materials, elastic anisotropy can lead to stress concentrations and inhomogeneities during plastic deformation.(Dieter, 1986) X-ray and neutron diffraction have been used extensively to determine the elastic constants (E_{hkl}, ν_{hkl}) for different crystallographic planes, in single crystals and polycrystalline materials.(Choo, Seo, Beddoes, Bourke, & Brown, 2004; Clausen et al., 1999; Rajagopalan, Little, Bourke, & Vaidyanathan, 2005) Such measurements are important for understanding the effects of anisotropy and texture on the macroscopic mechanical properties. Models and theoretical considerations can be found in past and recent literature, relating Young's modulus E and Shear modulus G to single crystal elastic constants.(Hill, 1952; Hutchings et al., 2005; Kröner, 1958; Nye, 1957; Singh, 2009)

A majority of the published experimental data associated with the lattice strain response of polycrystalline materials has been obtained using uni-axial tensile loading. In practical applications however, shear is often the predominant loading case and leads to dominant yield mechanism (Yu, 2002), but only a few detailed diffraction studies under direct application of shear stress have been carried out.(J. Bunn et al., 2010; Martins, Lienert, Margulies, & Pyzalla, 2005) Recently, Bunn et al. have shown that residual intergranular strains generated by the application of shear deformation behave differently than those generated by tensile deformation when explored on an ex-situ basis for hollow cylinders made from 12L14 steel alloy.(J. Bunn et al., 2010)

Experimental Setup

When isotropic solid cylinders are subjected to torsion within the elastic range, the maximum normal stresses (tensile and compressive) act at 45° to the longitudinal axis. The maximum shear stress and strain occur at the outer radius of the cylinder and are zero at its center.(Dieter, 1986; Martins et al., 2005) The maximum shear stress of a cylinder under torsion can be calculated as:

$$\tau = T \cdot \frac{r}{J}, \qquad (4.1)$$

where T is the applied torque, r is the radius and J the polar moment of inertia of the cylinder. In the case of pure shear, the magnitude of the principal strains on the surface of a cylinder relates directly to the magnitude of shear strain based on the strain rotation principle.(Bickford, 1998; Nye, 1957) During elastic deformation in torsion, it can further be assumed that plane sections perpendicular to the longitudinal axis of the cylinder remain plane and radial lines remain

straight.(Bickford, 1998; Young, 2002) Therefore no significant radial and circumferential strains and stresses are generated, thus the state of strain is two-dimensional (plane strain). Prior measurements by the authors at the Neutron Residual Stress Mapping Facility (NRSF2) at Oak Ridge National Laboratory (ORNL) and at the Residual Stress Analysis and Texture Diffractometer (E3) at Helmholtz Zentrum Berlin, using identical samples and setup as used in this study, confirmed that the strains in the radial, axial and circumferential direction of a cylinder remain small (within ±50 με, approximately the limits of measurement resolution) while the samples were elastically loaded in pure torsion to a maximum shear stress of 120 MPa.

In the present study, an experimental approach is reported using in-situ neutron diffraction for determining lattice plane (*hkl*) specific shear strains while subjecting a cylinder to a state of pure shear stress by torsional loading. The measurement principle and experimental requirements will be described in the first section of this letter. Then the method is illustrated by an example measurement at NRSF2, using a solid cylinder sample (d = 6 mm) made from a ferretic steel alloy (12L14), and results are reported. The presented technique allows probing shear strains within the interior of a sample, in contrast to other techniques, which are limited to the (near) surface, e.g. use of resistance based strain gauges(Perry, 1969), Digital Image Correlation(Chu, Ranson, & Sutton, 1985), Moiré Interferometry(Post, 1991), photo elastic methods(Zandman, 1961) and Electron Backscatter Diffraction (EBSD).(Wilkinson, Meaden, & Dingley, 2006)

For the neutron diffraction method described herein, *hkl* specific interplanar spacings (d_{hkl}) have to be measured for a given gauge volume in (at least three) independent directions, all lying in the "axial-circumferential" plane of the cylindrical sample, while incrementally subjecting the sample to pure torsion (within the elastic limit). The interplanar spacings are then

converted to strains using the d_{hkl} values measured at zero torque (d^0_{hkl}). The subset of grains within the neutron scattering gauge volume which are aligned such that the normal of the lattice plane is parallel to the diffraction vector are used as internal strain gauges to measure the *hkl* specific response to torsional shear. The principal strains (ϵ_1 and ϵ_2) and the maximum shear strain (γ_{xy}), at the measurement location, are calculated using the strain transformation suitable for a plane strain condition (Nye, 1957; Perry, 1969; Young, 2002), and the previously measured elastic strain components ($\epsilon_{\psi(hkl)}$):

$$\epsilon_\psi = \frac{\epsilon_x + \epsilon_y}{2} + \frac{\epsilon_x - \epsilon_y}{2}\cos(90° - \psi) + \frac{\gamma_{xy}}{2}\sin(90° - \psi) \qquad (4.2)$$

In order to measure the strain in three directions (three values of ψ yielding three ϵ_ψ) for a single spatial location within the solid cylinder, the loading system (Figure 4.1a) and therefore sample (Figure 4.1b) axis are inclined at angles between 0° and at 45° with respect to the horizontal (X-Y) plane defined by the incident and diffracted neutron beams. The highest sensitivity (i.e. lowest relative error) will be achieved at 45° where the lattice strains are at maximum. For the described experiment at NRSF2, the maximum inclination was limited to 41.3° due to interferences with slit holders. The derived shear strains are independent of the specific inclination used (authors have obtained similar results for an inclination of 31.5°), as long as the strains in that direction are non-zero.

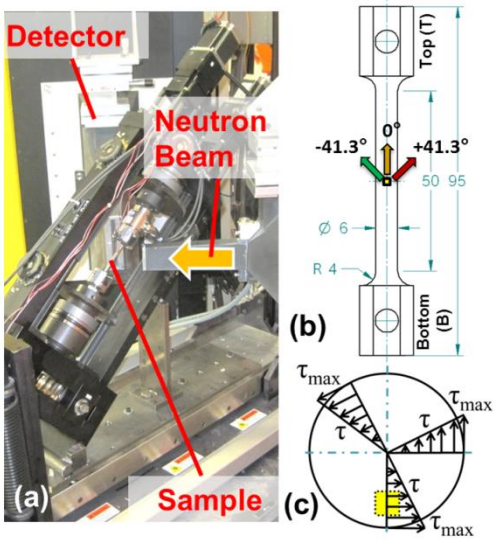

Figure 4.1 **(a)** Experimental setup at NRSF2 with loading system shown at 41.3° inclination **(b)** Sample dimensions (mm) and directions of measured strains at a gauge location 2 mm from the cylinder axis (B = bottom and T = top of sample) **(c)** Linear variation of shear stress along each radial line of the cylinder cross section with gauge location shown as yellow square.

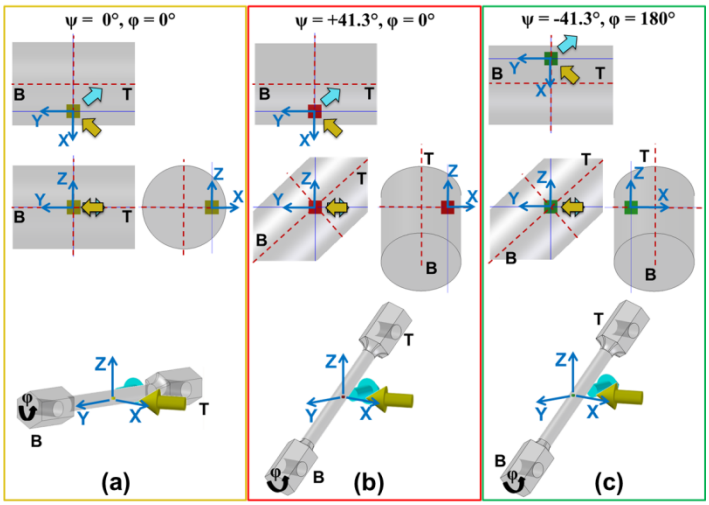

Figure 4.2 Sample positioning to obtain the three strain components **(a)** For ψ=0° the loading system is lying on its side, while **(b, c)** in the other two cases it is inclined at 41.3°. For measurement of the strain component corresponding to ψ=-41.3°, **(c)** the sample is rotated inside the loading system by 180° and the loading system is translated in x-direction, so the same spatial location within the sample is measured.

The gauge volume was positioned at a radial offset from the sample's cylinder axis as shown in Figure 4.1c and Figure 4.2 to ensure the gauge volume was fully within the cylindrical sample. In Figure 4.2, the yellow arrow represents the incident neutron beam; the cyan arrow represents the diffracted beam (the direction of measured strains bisects these two). The sample coordinate system is denoted by the dashed red lines and the instrumental coordinate system is shown in blue. The angle φ denotes the sample rotation inside the loading system. The gauge volumes are shown by yellow, red, green squares, respectively.

While inclining the loading system at 41.3°, one can measure the strain component corresponding to $\psi = +41.3°$ as well as $\psi = -41.3°$. To measure the latter, the sample is rotated inside the loading system by $\phi = 180°$ and the entire loading system is translated in the x-direction, such that the gauge volume resides at the same spatial location of the cylinder. It should be noted that measurement of the described strain components could also be achieved by rotating the sample stage (usually termed Ω) and without inclining the loading system, but for many diffraction instruments the range of rotation movement is typically restricted by slit/collimator interferences with the load frame.

In neutron diffraction, a volumetric averaging is used to achieve useful counting rates and grain averaging. However, to minimize impact of radial and circumferential variation of strains (for both see Figure 4.1c) the gauge volume has to be small compared to the sample dimensions. For the herein described experiments, the gauge volume (established by gadolinium slits) was chosen to be 1x1x1 mm^3. The impact of strain variation was explored using an even smaller gauge volume (0.7x0.7x0.7 mm^3), which resulted in much longer count times, with the conclusion that similar results were obtained. For the herein reported experiment, the gauge volume center was fixed at a radial distance of 2 mm from the axis of the sample. The shear

stress and strain at this location is 2/3 of the maximum shear stress and strain experienced on the surface of the cylinder. Due to the radial gradient of the shear stress/strain, a careful and precise alignment procedure is crucial in order to assure that the same gauge volume location is irradiated for each measurement condition. A positioning accuracy of the gauge volume location below 100 μm is required to achieve an uncertainty of < 5% in the calculated shear stress. The required accuracy was reached by using a laser alignment system, consisting of a FARO laser tracker and SScanSS software(Jonathan A. James & Edwards, 2007) to align the sample within 50 μm accuracy for gauge volume location. The gauge volume alignment procedure was repeated for every inclination of the loading system, prior to each loading experiment.

A portable axial/torsional loading system (Figure 4.1a) was utilized for the particular measurements, offering an axial force capacity of 50 kN, a torque capacity of 12 Nm and the ability to rotate a specimen under an applied load.(Woracek et al., 2011) The solid cylinder sample (Figure 4.1b) was machined from a hexagonal bar of low carbon BCC steel (12L14, Table 4.1). Significant strain gradients as function of radius were observed in an as-machined, unstressed sample. To relieve these internal stresses, the sample was annealed at 870°C for 15 minutes and slowly cooled. Using neutron diffraction, it was confirmed that the residual strain gradient for the stress-relieved sample was significantly reduced. Optical micrographs indicated a resulting average grain size of 25 μm. Texture measurements of the undeformed sample, carried out at the HIPPO instrument(Vogel et al., 2004) at Lujan Neutron Scattering Center (LANSCE), indicated mild to no bulk texture (Figure 4.3).

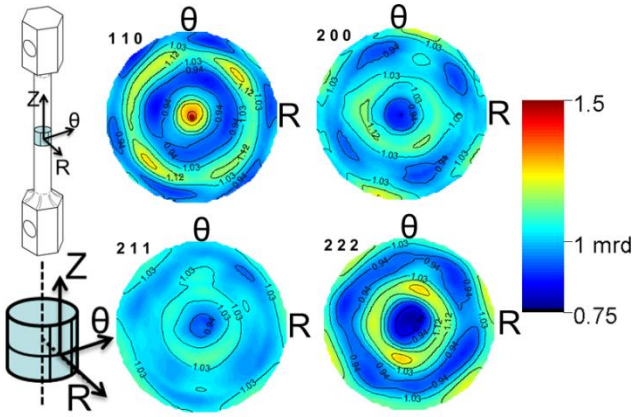

Figure 4.3 Pole Figures for stress relieved, un-deformed samples showing mild to no bulk texture.

An electrical resistance based rosette strain gauge was attached to the sample surface in the gauge section, 10 mm above the center to prevent interference with the incident neutron beam. The sample was connected to the load frame grips using a pin arrangement. Proper mechanical alignment of the sample in the load frame was verified by applying elastic loading in tension and torsion and calculating the principal strains. In the case of pure tension, shear strain γ_{xy} was observed to be essentially zero and for pure torsion, the out-of-plane bending strains were negligible.

Table 4.1 Chemical composition (weight percent) and mechanical properties of annealed (stress relieved) 12L14

C	*Mn*	*P*	*Pb*	*S*	Yield Strength [MPa] under Tension[a]	Shear Strength [MPa] under Torsion[a]
0.15 (max)	0.85 – 1.15	0.04 – 0.09	0.15 – 0.35	0.26 – 0.35	250	160

[a] Measured with portable loading system and verified separately with MTS servo-hydraulic loading system

Different neutron monochromator settings were used at NRSF2 to select the wavelength of neutrons. Changing the wavelength allowed investigation of several different lattice planes in the near 90° 2θ range. For the two strain components corresponding to a ψ value of +41.3° and -41.3°, neutron measurements were performed while applying a macroscopic shear stress between 0 MPa and 120 MPa, at 10 MPa increments. For ψ = 0°, measurements were performed only at 60 MPa increments, as the measurements are mainly used to verify proper load frame alignment. The axial stress was kept constant (using PID control) at a nominal tensile seating stress of 20 MPa for all measurements of shear stress. During data acquisition (10-40 minutes depending on investigated lattice plane) the angular twist and axial deformation were held at fixed positions. The reference interplanar lattice spacings d^0_{hkl} were determined at the same axial stress of 20 MPa and zero shear stress. The monochromator was changed following the loading/unloading cycles for a given hkl.

Results

The macroscopic surface principal strains and shear strains were monitored throughout the neutron diffraction experiments via the strain gauge rosette. Nearly identical macroscopic stress-strain behavior was seen in each loading/unloading cycle of the same sample and also for measurements on replicate samples. The macroscopic shear modulus under torsional loading was measured as 73 (± 1) GPa. No creep behavior was observed. The bulk average shear modulus predicted by the Reuss model is closest to the measured value (Table 4.2).

Table 4.2 Macroscopic values of shear moduli G [GPa] as calculated for α-Fe and experimentally determined (via strain gauge rosette) for 12L14.

α-Fe			**12L14**
acc. to Voigt(Hutchings et al., 2005)	acc. to Reuss(Hutchings et al., 2005)	acc. to Kröner(Hutchings et al., 2005)	Experimental
88.8	72.5	82.1	73 (± 1)

The strain components for three tilts for the bcc (211) plane, measured by neutron diffraction as a function of applied shear stress, are shown in Figure 4.4. The error bars represent the 2 x rms deviation of the determined strain values from four repeated loading experiments using the same sample. Note that strains $\epsilon_{+41.3^\circ}$ are positive (tensile), strains $\epsilon_{-41.3^\circ}$ are negative (compressive) and strains ϵ_{0° are essentially zero, as expected. Figure 4.4 also shows results obtained for spatial locations at a radial distance of r = 1 mm and the sample center (r = 0 mm). These additional data points confirm that the diffraction based measurements agree with the predicted radial variation of shear strain using elasticity theory. A significant change of lattice strain in the axial direction (ϵ_{0°) due to length change under application of (elastic) torsional stress(Young, 2002) was not observed.

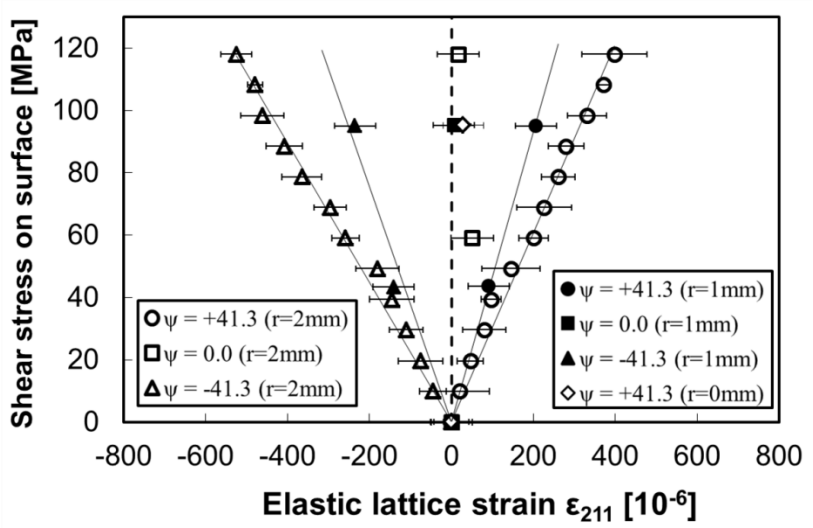

Figure 4.4 Measured strain components for ferritic bcc (211) lattice plane during elastic loading in torsion for three separate spatial locations along the same radial line (r = 2 mm, r = 1 mm, r = 0 mm). Shear stress corresponds to the maximum shear stress at the surface of the sample.

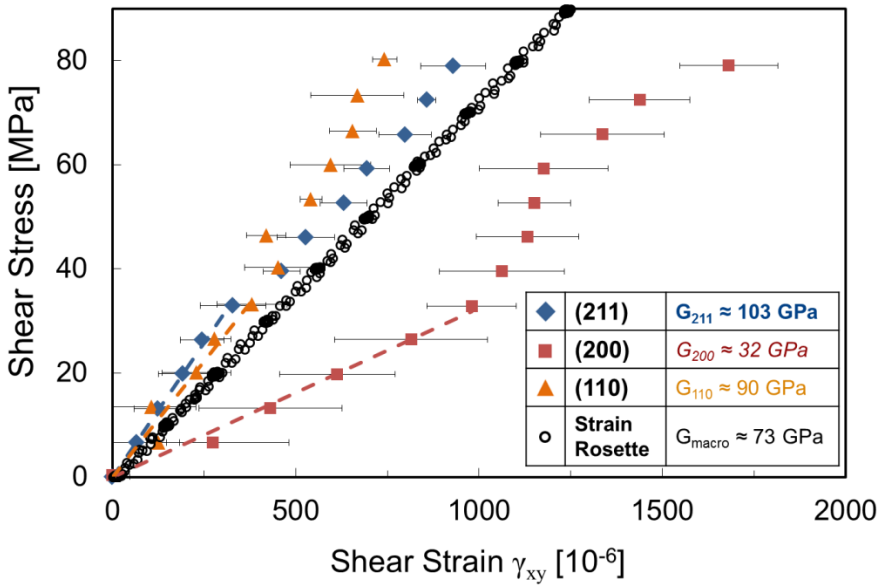

Figure 4.5 Shear Stress (at r = 2 mm for three *hkl's* and the surface for the strain rosette) *vs*. obtained Shear Strain (for the investigated lattice planes and strain rosette) with shear modulus ($G_{hkl} = \tau/\gamma_{xy}$) determined using a linear fit to the initial slope.

For the three measured strain components (ϵ_{0°, $\epsilon_{+41.3^\circ}$, $\epsilon_{-41.3^\circ}$), the shear strain can be obtained by using Equation 4.2 as

$$\gamma_{xy} = \frac{(\epsilon_{+41.3^\circ} - \epsilon_{-41.3^\circ})}{\sin 97.4^\circ}. \qquad (4.3)$$

The shear stress versus shear strain response is shown in Figure 4.5 for the three lattice planes. For bcc (200), it was observed that the shear stress *vs.* lattice strain response behaves non-linearly from about 40 MPa onwards, which typically indicates the onset of plastic flow, a feature also commonly observed in tensile mode(Clausen et al., 1999; Hutchings et al., 2005). A similar but much less pronounced shift is noticed from this figure for the other two *hkl's*. However, the non-linearity occurs at an unexpectedly low shear stress amplitude for all three *hkl's* (considering the macroscopic shear strength) and identical inference was observed for repeated loading cycles of the same sample for stress amplitudes well below yield stress in shear. Additionally, it appears that the bcc (200) planes start to soften again at approximately 60 MPa and this observation is perplexing and needs further investigation. The break in slope was not seen in the macro strain data from the attached strain gauge rosette where the surface shear strain response indicates perfectly linear elastic macroscopic strain behavior. It is further interesting to note that lattice strain data from a tensile test (which was performed using the same alloy, sample dimensions and setup; table 4.3) behaved perfectly linear.

Table 4.3 Calculated values of Young's moduli E_{hkl} and shear moduli G_{hkl} for α-Fe and experimentally determined E_{hkl} and G_{hkl} for 12L14.

Lattice Plane *hkl*	**α-Fe**		**α-Fe**		**12L14**	
	E_{hkl} [GPa] acc. to Reuss(Hutchings et al., 2005)	G_{hkl} [GPa] acc. to Reuss(Singh, 2009) [a]	E_{hkl} [GPa] acc. To Kröner(Hutchings et al., 2005)	G_{hkl} [GPa] acc. to Kröner/deWitt(Singh, 2009)	Experimental E_{hkl} [GPa] [b]	Experimental G_{hkl} [GPa]
bcc (211)	210.5	84.4	225.5	96.9	208	103
bcc (200)	125	46.3	173.3	70.8	146	32-50
bcc (110)	210.5	84.4	225.5	96.9	197	90

[a] Calculated using stiffness constants presented in (Hutchings et al., 2005) (page 220)

[b] Tensile measurements were performed using the same alloy, sample dimensions and setup, while subjecting the sample to axial stresses between 20 MPa and 100 MPa, at 10 MPa increments, and keeping the shear stress at 0 Mpa.

The shear moduli G_{hkl} was determined using linear regression between 0 MPa and ≈ 33 MPa shear, because of the non-linearity of the data based on lattice specific shear strains for stress amplitudes above 33 MPa. The shear moduli corresponding to the ferritic bcc (211) and bcc (110) planes are significantly larger than that for the bcc (200) (Table 4.3). Under tensile loading, the bcc (211) and bcc (110) planes show a similar order of stiffness and it appears that these two *hkl's* behave similarly for pure shear stress application under torsion. The crossover at about 40 MPa in Figure 4.5 for those two lattice planes cannot be fully rationalized at this stage due to relatively large error bars relative to the changes near the crossover. The bcc (200) planes are found to be much weaker under torsion than would be expected from tensile results, when comparing on a relative scale. The *hkl* specific Youngs's moduli E_{hkl} and Shear moduli G_{hkl} following the Reuss (stress continuity) and Kröner modeling schemes are presented in Table 4.3. The experimentally determined values for E_{hkl} are closer to the Reuss values than to the Kröner, but the experimentally determined G_{hkl} values for bcc (211) and bcc (110) are much closer to the

values predicted by Kröner/deWitt(Singh, 2009). For the bcc (200) plane however, it is difficult to interpret a single value of shear modulus due to the pronounced non-linearity starting at shear stress value of 40 MPa. Using the initial linear part of the slope, yields G_{200} to be 32 GPa, while linear regression of the entire data set yields a value of 50 GPa.

Repeatability Studies – Reflection Method

Due to the symmetry of the strains measured under simple shear, an additional assumption can be made in many cases. Because the $\epsilon_{+41.3^\circ}$ and $\epsilon_{-41.3^\circ}$ are symmetric about the zero line, it can be assumed that their magnitudes are similar and therefore that $\epsilon_{+41.3^\circ} = -(\epsilon_{-41.3^\circ})$. By using this assumption and the knowledge that ϵ_{0° is essentially zero only a single tilt is required for data analysis. This method is referred to as the reflection method.

An additional experiment is used to demonstrate the viability of this methodology and test the repeatability of shear moduli measured using the method detailed previously in this study. An identical sample as studied previously is used and the (110) plane selected for a repeatability analysis. Three cycles of elastic loading from 0-120MPa surface shear stress in steps of 10MPa and then subsequent unloading back to zero shear surface stress are performed. The frame is next tilted at $\psi = -41.5°$and for all cycles $\epsilon_{-41.3^\circ}$ is measured for the (110) plane. The measured strains and reflected data is shown in Figure 4.6. The measurements were taken with the gauge volume places at 2mm from center of the sample. Using the same analysis as used in the previous section, the shear moduli are obtained for the loading and unloading cycles measured before. Each load point is averaged over the three separate runs. Figure 4.7 compares the 3 different shear moduli, G_{hkl}, derived from the data. In all the cases the moduli are very repeatable (within 10%).

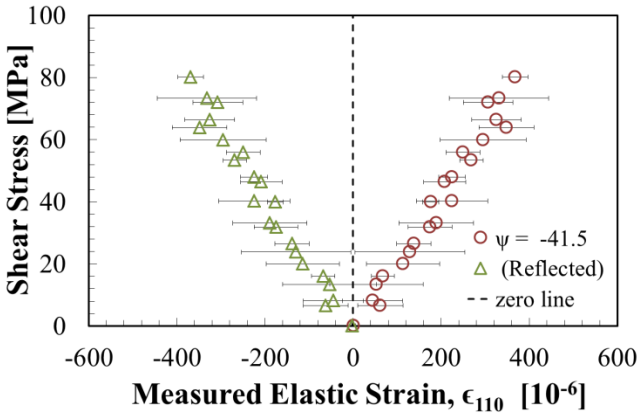

Figure 4.6 Measured strain components for ferritic bcc (110) lattice plane during elastic loading in torsion for multiple loading/unloading cycles at a radial offset of 2mm from center.

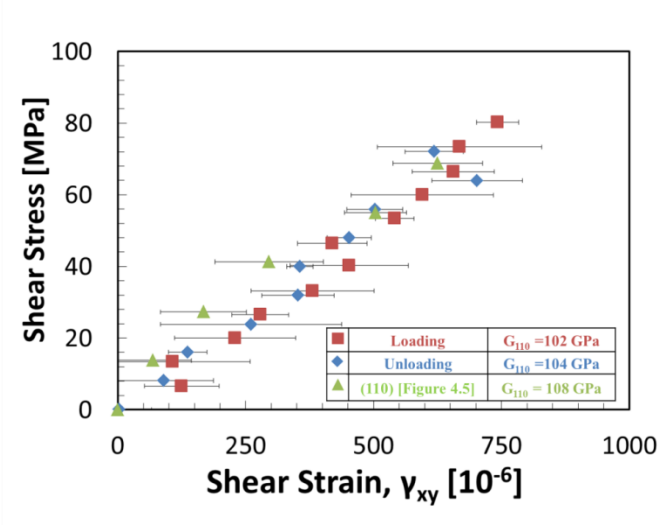

Figure 4.7 Shear stress at r = 2mm versus derived shear strain for the (110) reflection for repeatability runs performed as well as calculated shear moduli

Conclusions

This study presents a neutron diffraction method to obtain the lattice specific shear modulus of polycrystalline materials. The in-situ tests with ferritic 12L14 alloy confirmed the method. The 12L14 results are a first step in understanding effects of the application of shear stress on the mechanical behavior of polycrystalline materials and associated elastic anisotropy.

Results suggest that, when applying pure torsion within the elastic regime to a cylinder, it can be sufficient to measure only one strain component (close to 45°) and use the assumption of symmetry to calculate shear strain. The reflection method could therefore be a viable method to use on engineering diffractometers to save beam time without sacrificing measurement fidelity.

Initial results, obtained for 12L14 ferritic steel alloy, indicate that the (200) lattice planes show a different behavior under torsional shear than would be expected from properties determined under uni-axial tensile loading. The phenomenon of early onset of non-linearity in measured shear modulus due to direct application of shear stress will need to be studied in more detail for bcc materials and explored for polycrystalline materials with complex slip systems (fcc, hcp).

The described experiments were performed at a high flux steady state neutron source, however there are potential advantages to conduct future experiments at pulsed sources with adequate spatial resolution. This can be particularly advantageous for exploring plastic and time dependent strain (while the need of measuring more strain components must be considered for correct interpretation of the strain tensor in this case).

CHAPTER 5. IN SITU TENSOR EVOLUTION FOR 12L14 STEEL ALLOY EXPOSED TO COMBINED TENSION AND TORSION

Abstract

An experimental method to measure the full strain tensor evolution, using *in situ* neutron diffraction, is detailed. The methodology allows for the measurement specific polycrystalline *hkl* crystallographic planes' responses to applied proportional loading achieved in a combination of axial stress (tension) and shear stress (torsion) simultaneously. To establish the method, a pure bcc ferretic alloy (12L14) is measured. The bcc (211) full tensor response is measured under multiple elastic load steps.

Introduction

The traditional methodology for measurement of residual strain is to measure three strains orthogonal to one another at each mapping point. Previous studies have shown that while these directions are usually chosen for convenience of measurement (axial, radial, and hoop for example in a cylinder), the state of strain within a sample exists as a rank 2 symmetric tensor, which means that the principal strain is not necessarily aligned with one of these orthogonal directions. The author has explored this previously (J. Bunn et al., 2010). An *ex situ* study has also been performed on the same samples to capture a full tensor evolution (J. Bunn, Penumadu, Lou, & Hubbard, 2014) using the generalized least squared methodology proposed by Winholtz and Cohen (R. Winholtz & Krawitz, 1995; R. A. Winholtz & Cohen, 1988).

An earlier study by the authors has shown that with the assumption that in simple shear no radial strains are generated, *hkl* specific shear moduli and shear strains corresponding to specific crystallographic planes can be determined from the d-spacing response obtained through neutron diffraction experiments on a sample subjected to simple shear. In this method only a simple tilt of the load frame out of the plane of diffraction is required. The axial orientation is not

needed. This is because in simple shear no radial or axial stresses are generated in in elastic loading (R. Woracek, J. Bunn, D. Penumadu, & C. Hubbard, 2012). This technique has proven very powerful. However, if a combined torsion and tension loadings are to be studied then a complete tensor must be measured and the assumptions used in the Woracek, Bunn et al study will no longer apply. This is due to the fact that combined loading through simultaneous application of tension and torsion will produce strains in the axial and radial direction. Therefore at least six independent rotations of ϕ and ψ must be performed and the generalized least squared method used.

The rotations of ϕ and ψ must be obtained similar to the *ex situ* study, but a Huber orienter is no longer able to be used as now an entire load frame needs to be mounted. This presents many challenges with alignment, gauge volume shadowing from components and even instrument collisions. The load frame detailed previously is used in this study, with the specialized tilt mechanism used.

The laser tracker system in conjunction with SScanSS is the only possible option for the measurements. The only engineering neutron diffractometer with small enough gauge volume capability to measure cylinders of 6-10 mm with precision is the Neutron Residual Stress Facility (NRSF2) at the High Flux Isotope Reactor (HFIR)(Cornwell et al., 2012; J. A. James et al., 2008; Oak Ridge National Laboratory, 2009; Tang & Hubbard, 2006).

The proposed complex loading state is achieved by the simultaneous application of tension through axial deformation and shear through torsion. To achieve this, the custom tension/torsion load frame which has been developed at the University of Tennessee is utilized.

The proportional loading factor, S_f, is always maintained between the applied axial stress and the applied shear stress ($S_f = \tau/\sigma$). In mechanics the stress factor is related to the rotation of the applied principal stress, β:

$$\boldsymbol{\beta} = \frac{\tan^{-1}\left(2\frac{\Delta\tau}{\Delta\sigma}\right)}{2} = \frac{\tan^{-1}(2S_f)}{2} \qquad (5.1)$$

Experimental Setup

In the study, a known combination of tensile and shear stress is applied to a 6 mm solid cylindrical sample (Figure 4). The sample is machined from 12L14 alloy steel, the same as used in the previous experiments: a single phase bcc ferretic steel alloy.

The custom tension/torsion frame mentioned previously is extremely well suited to perform these measurements. The frame has been utilized at multiple neutron facilities worldwide. It is small in size, which is ideal for the rotations that are needed. The frame's axial force capacity is 0-50 kN and has a torque range of 0–12 Nm.

Due to the gradient of shear strain versus radius of a cylinder, a cubic 1mm x 1mm x 1mm gauge volume is needed to reduce smearing across the gradient. The gauge volume center is placed at a radial position 2mm from the center of the sample as in previous studies (Figure 5.2). To maintain the position of the gauge volume within the sample, both the top and bottom grips are rotated in opposite directions to generate a desired torque. This technique also allows the gauge volume remain over the same subset of grains throughout the experiment.

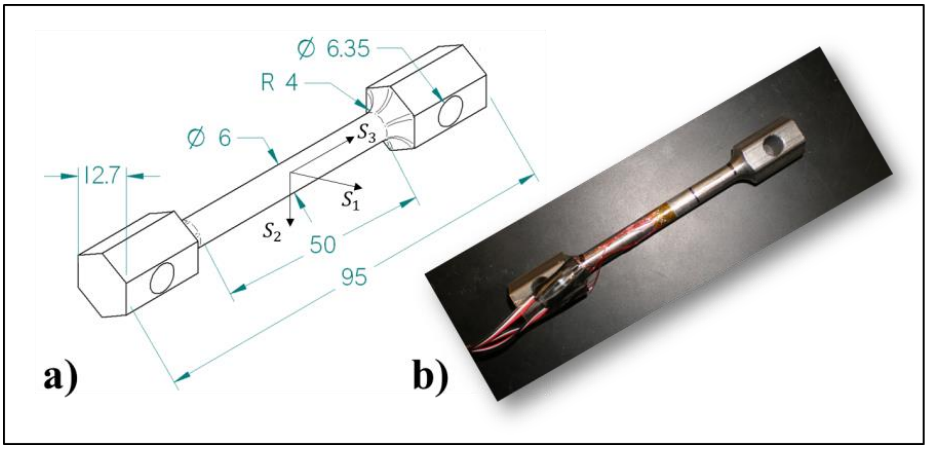

Figure 5.1 **a)** Sample dimensions (mm) and defined sample coordinate system for the solid cylinder used in the *in situ* experiments and **b)** image of the sample with surface mounted strain gauge.

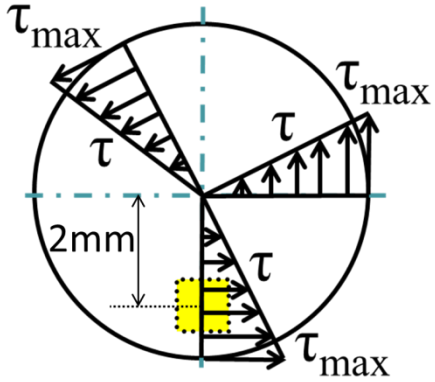

Figure 5.2 Cross section showing shear stress gradient with radial position, and experimental gauge volume location (Robin Woracek et al., 2012)

For each loading step, as the shear stress increases the tensile stress will increase proportionally. In the study a $\beta = 30°$ is to be maintained (based on $\tau_{surface}$). The actual rotation experience at the at the neutron measurement location (r = 2mm) will be $\beta \approx 24°$ due to the decreased in shear stress along the radial direction moving toward the sample center.

The elastic d-spacing response, d_{hkl}, is measured at the combinations of ϕ and ψ as shown in Table 5.1 for 7 loading steps. Each loading point will be repeated three times to achieve a

better statistical average. Due to the number of independent rotations of the frame needed, and increased neutron count time for a 1mm x 1mm x 1mm gauge volume, only a single crystallographic lattice will be explored. The (211) is chosen because it has been shown to be insensitive to intergranular strains and has the best observed neutron counts versus background (J. Bunn et al., 2010; J. Bunn et al., 2014; J. R. Bunn et al., 2013; Hutchings et al., 2005). Also the (211) best represents the macro response of the material in both pure tension and pure torsion.

Table 5.1 Table detailing the various rotations of ϕ and ψ at which $\epsilon_{\phi\psi}$ is measured

ϕ	ψ
0.0°	-25.1°
5.5	-25.1°
0.0°	-31.6°
5.7°	-31.6°
0.0°	31.6°
-9.3°	31.6°
0.0°	-41.3°
-10.6°	-41.3°
0.0°	41.3°
6.4°	41.3°
0.0°	0.0°
0.0°	90.0°
-14.9°	90.0°

To perform each measurement the entire load frame assembly must be rotated. However unlike in the previous *ex situ* measurements a Huber orienter cannot be used due to the size and weight of the load frame. No tilt stage capable of tilting the load frame in multiple values of ψ automatically out of the plane of diffraction exists at NRSF2. Therefore the use of the laser

tracker and SScanSS must be used in order to repeatably measure the sample point in the sample coordinate system over multiple manual tilts of ψ.

In the experiment, five separate tilts of ψ are needed. The rotations of 0° and 90° are readily achieved as they represent the frame mounted horizontally and vertically. The tilts of ±41.3°, ±31.6° and 25.1° are achieved with a manual wedge-tile assembly. Figure 5.3 shows the frame mounted at a tilt of 31.6° with the incident snout of the neutron diffractometer removed for clarity. Movement of the wedge supporting the frame will yield multiple discrete tilts of the load frame assembly. The tilt can then be precisely determined by the use of the laser tracker.

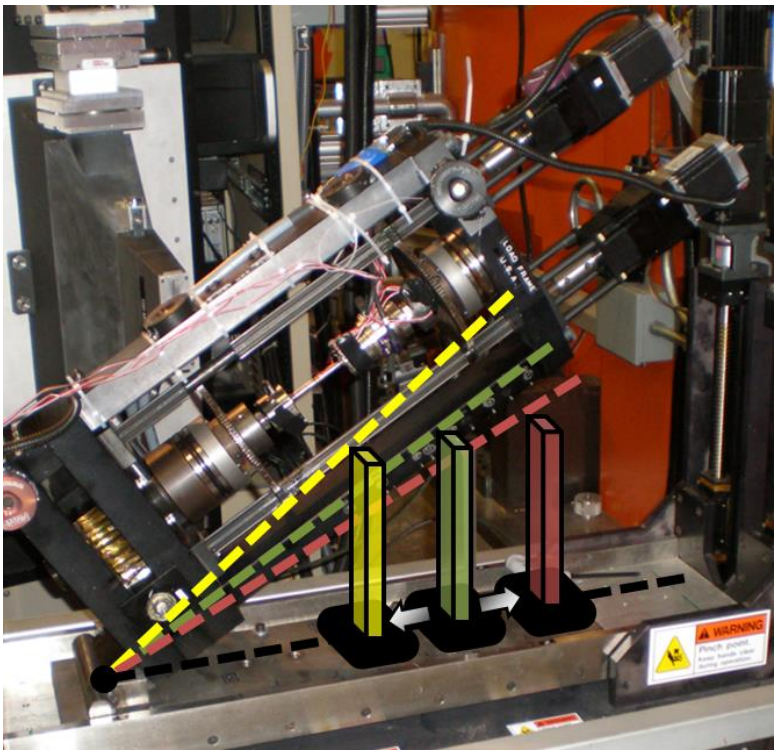

Figure 5.3 Load Frame tilted at 31.6°. By movement of the manual wedge tilts of higher degree (yellow) and lower degree (red) can be achieved.

To achieve greater fidelity in measurement, negative values for ψ are desired. However, it is not possible to tilt the frame in the opposite direction and perform diffraction measurements. To achieve a negative value for ψ rotation the sample is rotated within the load frame by rotating both grips simultaneously. Next the gauge volume is moved to the opposite side of the cylinder to the same set of grains for the positive tilts. This effectively gives a negative value of ψ rotation with a positive tilt of the load frame. A sketch detailing this transformation is shown in Figure 5.4.

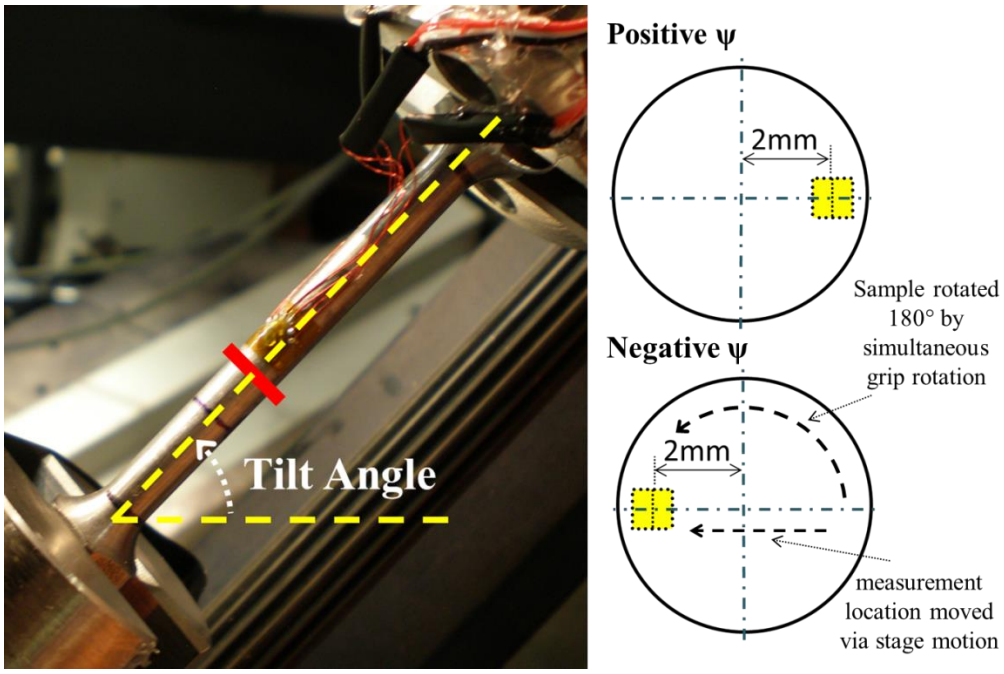

Figure 5.4 Sketch detailing the measurement of negative values of ψ for the same gauge volume of grains while maintaining the same tilt angle

Repeated alignment of the sample gauge volume at the same subset of grains at each tilt value and throughout elastic sample loading is an absolute necessity for the experiment to be successful. The laser tracker system at NRSF2 is uniquely situated to perform this alignment. The system utilizes SScanSS, a virtual laboratory system, to align the gauge volume

with an accuracy of less than 100µm. The process of which is detailed previously. In general the process utilizes the measurements of fiducial points in two coordinate systems (sample coordinate system and instrument coordinate system). The points are then iteratively combined and the resulting coordinate system transformation is applied to the desired measurement point(s). A simple graphic detailing this is shown in Figure 5.5.

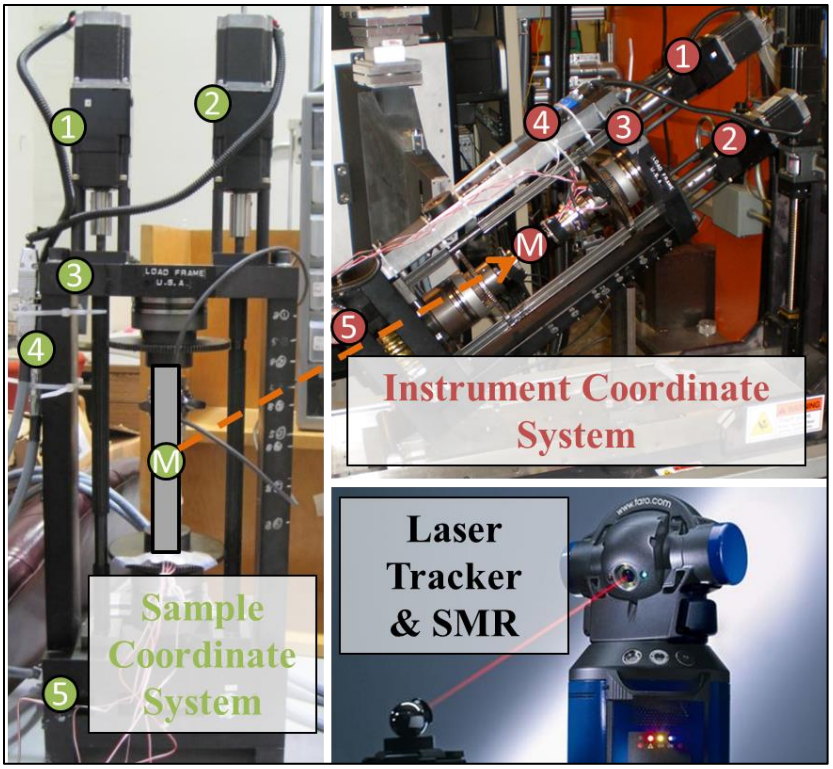

Figure 5.5 Photo of the FARO laser tracker at NRSF2 and the SMR used to measure fiducial points. Graphic detailing how points measured offline in the sample coordinate system are measured again in the instrument coordinate system (Pts 1-5). The measurement point (M) is then transformed into the instrument coordinate system (FARO, 2014)

Results

Multiple tilts and corresponding $d_{\phi\psi}$ values are measured successfully. The corresponding datasets are processed using a MATLAB code used in previous published studies to perform the generalized least squared method.

The resulting strain tensors for each load step are calculated for the proportionally increased loading. The data for each load step is presented in Figure 5.6 in the form of Mohr's circles. As expected, with each increasing load step the Mohr's circle expands. Due to the chosen coordinate system the expansion corresponds to increasingly negative normal strain (tension). As expected the minimum strain, ϵ_3, is controlling. This is evident from the only small difference between ϵ_2 and ϵ_1. The applied octahedral shear stress and corresponding principal strains are calculated in this same process and the relationship between the two is displayed in Figure 5.7. Again note the controlling strain being that of the minimum principal strain with a Poisson effect seen in ϵ_1.

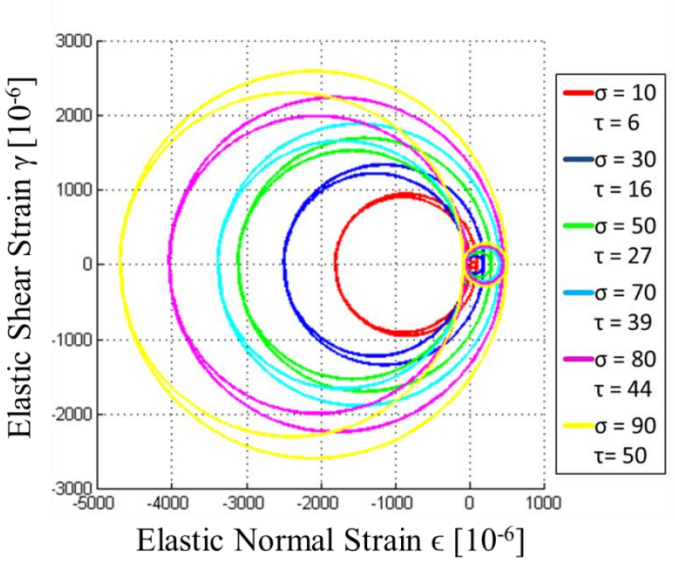

Figure 5.6 Plot showing the state of strain for each loading step in Mohr's space.

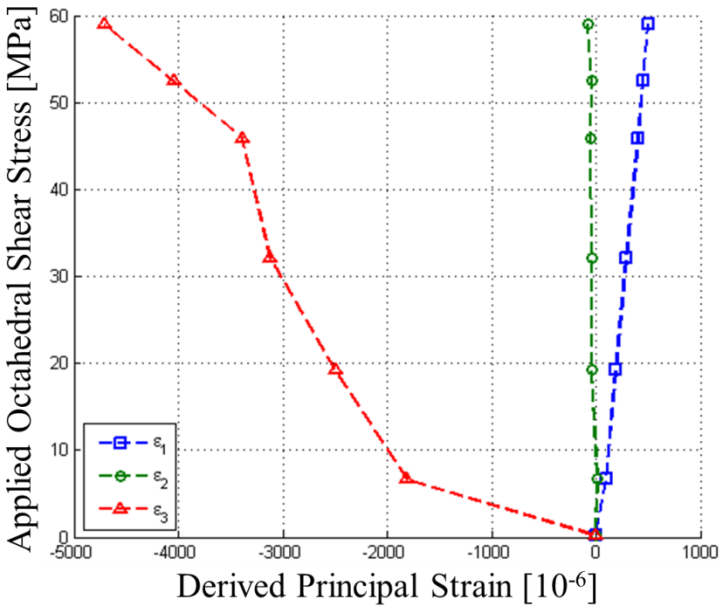

Figure 5.7 Applied Octahedral Shear Stress versus the calculated principal strain for the generalized least squared method

A point was made in the experiment to always maintain a similar rotation of β, the rotation of the principal strain. The rotation of the principal strain in the experiment is calculated from the full tensor analysis. This value is referred to as $\beta_{derived}$. The value is calculated for all load steps and compared to the rotation applied, $\beta_{applied}$, for each load step. The $\beta_{applied}$ is the rotation assumed from the applied axial stress and shear stress at 2 mm from the center (gauge volume location). As seen in Figure 5.8, good agreement is seen between $\beta_{applied}$ and $\beta_{derived}$.

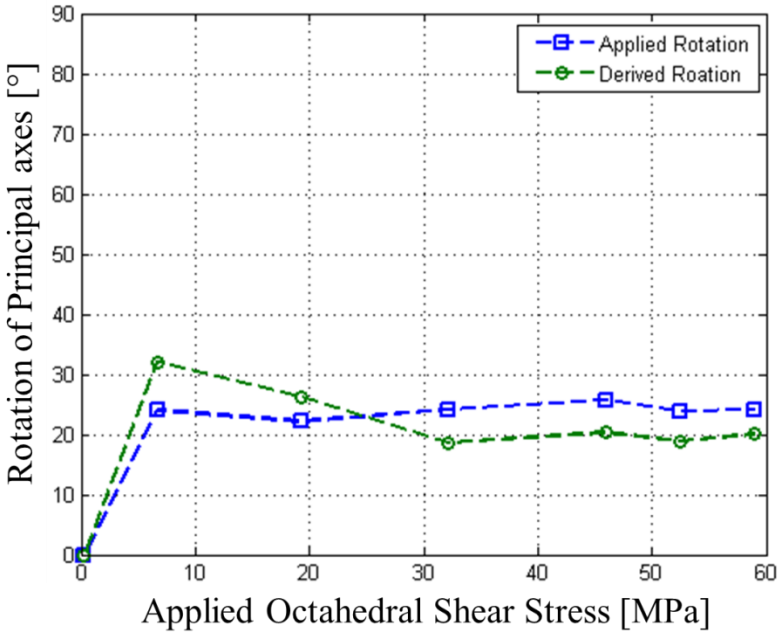

Figure 5.8 Derived and applied rotations of the principal axes versus the octahedral stress stress for each load step

Discussion and Conclusions

The first successful measurement of a crystallographic full strain response *in situ* of a cylindrical sample exposed to both tension and torsion simultaneously is demonstrated in this study. The experimental results are primarily proof of concept. However, some points for discussion are evident in the outcome. Because the rotations of the principal strain applied versus the rotations calculated from the neutron measured strain tensor, a higher level of confidence exists in the methodology.

The proof of concept results are based upon the bcc (211) planes in a 12L14 alloy. This plane best represents the macro response of the material. Therefore multiple models of yield could be explored using the new state of strain approach shown in the study. The (211) plane

would be helpful in an applied case for looking at complex state of yield in engineering parts that experience combined loading through various load paths.

Additional crystallographic planes should be explored to observe the effect complex loads will have on individual *hkl* lattice elastic responses. One can expect that based on the previous studies of the author that a high level of load path dependence must exist (J. Bunn et al., 2010; J. Bunn et al., 2014; Robin Woracek et al., 2012). With an increasing level of knowledge about the lattice specific responses of multiple crystallographic planes within a material a better understanding of a complex yield mechanism is achievable.

The measurements are time consuming, difficult to perform, and only are achievable currently at NRSF2. This is due to the integration of the UTK portable tension/torsion frame, the small gauge volumes the instrument provides, the flux of HFIR, and the expertise needed to perform the measurement. Currently it is reasonable to assume that this level of analysis is not going to reach the mainstream level of traditional residual stress mapping. However, it is very well suited to the exploration of high penalty of yield engineering components such as those in aerospace and nuclear engineering.

CHAPTER 6. SUMMARY AND FUTURE WORK

Summary

In this research, the development of new methodologies for both neutron and x-ray diffraction are used to explore engineering materials' responses to shear load through pure torsion and complex loadings such as combined proportional loadings and how those responses vary when compared to the traditionally measured response to uniaxial tension.

Samples of a bcc steel alloy are subjected to a known amount of large plastic deformation in two different deformation paths. One is deformed in pure torsion and the other in uniaxial tension. With the use of the engineering diffractometer NRSF2 at HFIR, residual strains corresponding to three crystallographic planes – the (211), (110), and (200) – are mapped along the radius and in three orthogonal orientations (axial, radial, and hoop). Gradients of residual strain are observed in all samples. Two approaches for the measurement of the unstressed lattice spacing are used. The stress free approach uses a powder to define d^0_{hkl}. In this case large gradients along the radius are observed and attributed to effects remaining from machining of the samples. The initial state approach normalizes the strains measured versus a cylinder that is as-received with no additional deformations. This approach yields any strains resultant from the large plastic deformations. In this case it is clear to see that different applied load paths lead to different resulting states of residual strain. It is demonstrated while some crystallographic planes are sensitive to intergranular strains resulting from applied tension; no indication of sensitivity can be seen for the application of torsion. The study sufficiently shows that residual strains' sensitivity to plastic deformation depends on the mode of applied deformation. It is clear that two different modes of plastic deformation that generate the same octahedral shear strain invariant do

not necessarily generate similar sensitivity in residual strain measurements that can be seen through only three orthogonal measurements.

As an expansion on previous experiments the same cylindrical samples are mounted to a Huber orienter and diffraction measurements are performed for multiple combinations of ϕ and ψ rotations. With this technique, precise alignment using NRSF2's laser tracker system is needed to achieve a precise placement of the gauge volume at the center of each rotation axes. With the values of d-spacing measured at the rotations of ϕ and ψ a least squared analysis is performed to solve for the general strain tensor. With the general strain tensor, no longer is the data limited to only three directions of strain measured. With the tensor, strain in any direction can be ascertained, as well as principal strains and directions computed. Comparing the invariants of the differing load paths show that they in fact do not behave similarly in all planes. The sensitivity in loading path can be deduced and quantified using this methodology.

A new experimental method to attain shear strain of specific crystallographic lattices (*hkl*) is developed and demonstrated for a simple bcc material. The measurements are obtained through loading a solid cylindrical sample in pure torsion. The measure is obtained within the bulk of the material along the radius in which a linear shear stress versus radius gradient exists. The measurements utilize the same simple bcc 12L14 ferretic steel alloy which has been studied previously. The method uses a custom tension/torsion load frame developed specifically for use on neutron instruments. The precise placement of the gauge volume upon tilting of the load frame out of plane is achieved through NRSF2 trackers in a first ever application of this accuracy and precision. Without the small gauge volumes provided by NRSF2 and the laser tracker/SScanSS integration, these measurements would not be possible. The shear strain responses of the same three crystallographic planes measured previously – (211), (110), and

(200) – are obtained within the polycrystalline sample. The first ever measured *hkl* specific shear moduli are reported. Results of the study indicate that a varied degree of anisotropy result from torsional loading of shear than those seen previously in tensile loading.

An experimental methodology to measure strain tensor evolution in polycrystalline materials with load using *in situ* neutron diffraction is performed. The first ever *in situ* neutron measurement of a crystallographic plane's response to the application of a complex proportional load is demonstrated. The proportional loading is achieved through the application of tensile stress and the application of shear through torsion. This study is performed to devise a methodology for the repeatable measure of the general strain response *in situ* to any state of applied elastic deformation. The technique is performed and verified against expected outcomes. The rotation of the principal strain that is applied for each step of proportional loading agrees well with the derive rotation of the calculated strain tensor. As these experiments are time consuming and difficult to perform, they would most like be best served on high penalty of yield of engineering components.

Future Work

Future expansion of this work that could be performed should include:

- *Ex situ* measurement of a full strain tensor utilizing a time of flight (TOF) diffractometer such as VULCAN at ORNL or SMARTS at the Lujan Center at Los Alamos National Lab (LANL). With this increased fidelity of multiple (*hkl*) planes' responses a better understanding of what the mechanisms underlying the load path dependence demonstrated are and how they could be either mitigated or exploited for design.

- Expansion of the *ex situ* measurements of a full strain tensor of a more complex slip system seen commonly in engineering material such as a fcc or hcp structure. With aluminum and magnesium becoming more common as structural materials a better understanding of any load path dependence that may exist in these more complex slip systems would be of high impact to design of future engineering components
- This research has stretched the measurement capabilities of world class diffraction facilities. It has demonstrated needs for:
    1. The precise alignment systems that go beyond optical gauge volume placement such as the FARO laser trackers present at NRSF2 and the SScanSS software in development for engineering diffractometers around the world.
    2. Smaller gauge volumes alongside their more precise placement. The gauge volumes achievable at NRSF2 are some of the smallest available due to the system designed for definition of these gauge volumes and the flux provided by HFIR, one of the highest flux reactor neutron sources in the world.
    3. Load frames capable of loading a sample in tension as well as torsion. These frames need to be robust enough to test a majority of engineering materials, yet small enough to fit within the space constraints presented by engineering diffractometers
    4. The ability to reliably tilt these load frames out of the plane of diffraction. Most load frames are designed such that they will only measure either on their side or vertical. For the measurement of the general state of strain a frame should be able to be tilted at multiple values between 0° and 45°.

- The application of the method to determine shear response of (*hkl*) crystallographic planes and their corresponding crystallographic shear moduli, the elastic constant G_{hkl}. This is an amazing opportunity to measure an additional elastic constant in a polycrystalline material. With this additional information a wealth of continuum mechanics can be directly applied for design of components fail as a result of complex loadings.
- Another step forward is to study effect of complex loadings on creep or on fatigue. With new pulsed instruments like VULCAN, stereoscopic measurements of multiple rotations can be attempted along with fatigue applied along multiple axes of loading simultaneously using the specialized MTS load frame present at VULCAN. This is no doubt an ambitious undertaking, but can yield very actionable results with respect to life cycle analysis of parts exposed to complex states of fatigue loading, such as aerospace alloys.

LIST OF REFERENCES

Allen, A. J., Hutchings, M. T., Windsor, C. G., & Andreani, C. (1985). NEUTRON-DIFFRACTION METHODS FOR THE STUDY OF RESIDUAL-STRESS FIELDS. *Advances in Physics, 34*(4), 445-473.

Bickford, W. (1998). *Advanced mechanics of materials*. Menlo Park, CA: Addison-Wesley.

Bragg, W. H. (1913). The Reflection of X-rays by Crystals. (II.). *Proceedings of the Royal Society of London. Series A, Containing Papers of a Mathematical and Physical Character, 89*(610), 246-248. doi: 10.2307/93487

Bragg, W. H., & Bragg, W. L. (1913). The Reflection of X-rays by Crystals. *Proceedings of the Royal Society of London. Series A, 88*(605), 428-438. doi: 10.1098/rspa.1913.0040

Brown, D., Bourke, M., Tomé, C., Varma, R., Holden, T., & Clausen, B. (2003). A neutron diffraction and modeling study of uniaxial deformation in polycrystalline beryllium. *Metallurgical and Materials Transactions A, 34*(7), 1439-1449.

Bunn, J., Penumadu, D., & Hubbard, C. (2010). Residual strain evolution in steel samples: tension versus torsion. *Applied Physics A, 99*(3), 571-578. doi: 10.1007/s00339-010-5616-1

Bunn, J., Penumadu, D., Lou, X., & Hubbard, C. (2014). Effect of Multi-Axial Loading on Residual Strain Tensor for 12L14 Steel Alloy. *Metallurgical and Materials Transactions A*, (Accepted March 2014).

Bunn, J. R., Penumadu, D., Woracek, R., Kardjilov, N., Hilger, A., Manke, I., & Williams, S. (2013). Detection of water with high sensitivity to study polymer electrolyte fuel cell membranes using cold neutrons at high spatial resolution. *Applied Physics Letters, 102*, 234102.

Chen, P. C., & Oshida, Y. (1989). *RESIDUAL-STRESS ANALYSIS OF A MULTI-LAYER THIN-FILM STRUCTURE BY DESTRUCTIVE (CURVATURE) AND NON-DESTRUCTIVE (X-RAY) METHODS* (Vol. 153).

Choo, H., Seo, D., Beddoes, J., Bourke, M. A. M., & Brown, D. W. (2004). In situ neutron diffraction studies on the elevated-temperature deformation behavior of a TiAl?W alloy. *Applied Physics Letters, 85*(20), 4654-4656.

Chu, T., Ranson, W., & Sutton, M. (1985). Applications of digital-image-correlation techniques to experimental mechanics. *Experimental Mechanics, 25*(3), 232-244. doi: 10.1007/bf02325092

Chung, D. H., & Buessem, W. R. (1967). The Elastic Anisotropy of Crystals. *Journal of Applied Physics, 38*(5), 2010-2012.

Clausen, B., Lorentzen, T., Bourke, M. A. M., & Daymond, M. R. (1999). Lattice strain evolution during uniaxial tensile loading of stainless steel. *Materials Science and Engineering: A, 259*(1), 17-24. doi: 10.1016/s0921-5093(98)00878-8

Cornwell, P. A., Bunn, J. R., Schmidlin, J. E., & Hubbard, C. R. (2012). Laboratory Guide for Residual Stress Sample Alignment and Experiment Planning-October 2011 Version (pp. Medium: ED).

Cullity, B., & Stock, S. (2001). Elementary of X-ray Diffraction. *Englewood Cliffs, 3rd*.

Cullity, B. D. (1978). *Elements of X-Ray Diffraction* (2nd ed.). Reading, MA: Addison-Wesley.

Davydov, V., Lukas, P., Strunz, P., & Kuzel, R. (2009). Evolution of internal stresses in the plain ferritic steel studied by neutron diffraction in situ upon tensile straining. [Article]. *Journal of Physics-Condensed Matter, 21*(9). doi: 095407

10.1088/0953-8984/21/9/095407

Daymond, M. R., & Priesmeyer, H. G. (2002). Elastoplastic deformation of ferritic steel and cementite studied by neutron diffraction and self-consistent modelling. *Acta Materialia, 50*(6), 1613-1626.

Dieter, G. E. (1986). *Mechanical Metallurgy* (Third Edition ed.). New York, NY: McGraw-Hill.

Eringen, A. C. (1980). *Mechanics of Continua (2nd edition ed.)*: Krieger Pub Co.

FARO. (2014). FARO Product Overview - 3D and Beyond, 2014, from http://www.faro.com/en-us/products

Ford, H. (1963). *Advanced Mechanics of Materials*. London: Longmans.

Hill, R. (1950). *The Mathematical Theory of Plasticity*. Oxford: Clarendon Press.

Hill, R. (1952). The Elastic Behaviour of a Crystalline Aggregate. *Proceedings of the Physical Society. Section A, 65*(5), 349.

Hutchings, M. T., Withers, P. J., T.M.Holden, & Lorentzen, T. (2005). *Introduction to the Characterization of Residual Stress by Neutron Diffraction*. Boca Raton, FL: CRC Press.

James, J. A., & Edwards, L. (2007). Application of robot kinematics methods to the simulation and control of neutron beam line positioning systems. *Nuclear Instruments and Methods in Physics Research Section A: Accelerators, Spectrometers, Detectors and Associated Equipment, 571*(3), 709-718. doi: 10.1016/j.nima.2006.11.033

James JA, O. E., Paradowska A, Hubbard CR, Schmidlin JE, Edwards L. (2008). Robotics Methods for Beam Line Instrument Simulation and Control.

James, J. A., Oliver, E. C., Paradowska, A., Hubbard, C. R., Schmidlin, J. E., & Edwards, L. (2008). *Robotics Methods for Beam Line Instrument Simulation and Control*.

James, J. A., Santisteban, J. R., Edwards, L., & Daymond, M. R. (2004). A virtual laboratory for neutron and synchrotron strain scanning. [Article]. *Physica B-Condensed Matter, 350*(1-3), E743-E746. doi: 10.1016/j.physb.2004.03.194

Joffe, A. F. a. K., M.V. (1922). Röntgenograms of strained crystals. *Philosophical Magazine, 43*, 204-206.

Krawitz, A. D., Brune, J.E., Schmank, M.J., . (1981, July 1981). *Measurement of Stress in the Interior of Solids with Neutrons*.

Kröner, E. (1958). Berechnung der elastischen Konstanten des Vielkristalls aus den Konstanten des Einkristalls. *Zeitschrift für Physik A, 151*(4), 504-518. doi: 10.1007/bf01337948

Larsson, C., Clausen, B., Holden, T., & Bourke, M. (2004). Measurements and predictions of strain pole figures for uniaxially compressed stainless steel. *Scripta Materialia, 51*(6), 571-575.

LeMaster, R., Boggs, B., Bunn, J., Hubbard, C., & Watkins, T. (2007). Grinding Induced Changes in Residual Stresses of Carburized Gears. *Lateral, 4*, 3.

Lemaster, R. A., Boggs, B. L., Bunn, J. R., Hubbard, C. R., & Watkins, T. R. (2009). Grinding Induced Changes in Residual Stresses of Carburized Gears. *Journal Name: Gear Technology, The Journal of Gear Manufacturing; Journal Volume: 26; Journal Issue: 2*, Medium: X; Size: 41-49.

Lester, H., & Aborn, R. (1925). Behaviour under stress of iron crystal in steel. *Army Ordnance, 6*, 120.

Malvern, L. E. (1969). *Introduction to the mechanics of a continuous medium*. New Jersey: Prentice-Hall, Inc.

Marin, T., Dawson, P. R., Gharghouri, M. A., & Rogge, R. B. (2008). Diffraction measurements of elastic strains in stainless steel subjected to in situ biaxial loading. *Acta materialia, 56*(16), 4183-4199. doi: http://dx.doi.org/10.1016/j.actamat.2008.04.048

Martins, R. V., Lienert, U., Margulies, L., & Pyzalla, A. (2005). Determination of the radial crystallite microstrain distribution within an AlMg3 torsion sample using monochromatic synchrotron radiation. *Materials Science and Engineering: A, 402*(1-2), 278-287. doi: DOI: 10.1016/j.msea.2005.04.005

Mase, G. E. (1970). *Continuum Mechanics* (2nd Edition ed.): McGraw-Hill Professional.

Meyers, M. A., & Chawla, K. K. (1984). *Mechanical Metallurgy: Principles and Applications*. Englewood Cliffs, N.J. 07632, U.S.A: Prentice-Hall, Inc.

Noyan, I. C., & Cohen, J. B. (1986). *Residual stress*.

Noyan, I. C., & Cohen, J. B. (1987). *Residual Stress, Measurement by Diffraction and Interpretation*: Springer, New York.

Nye, J. F. (1957). *Physical Properties of Crystals: Their Representation by Tensors and Matrices*: Clarendon Press.

Nye, J. F. (1985). *Physical properties of crystals: their representation by tensors and matrices*: Clarendon Press.

Oak Ridge National Laboratory, N. S. (2009). Instrument Systems Descriptions at HFIR: HB-2B Retrieved 10 July, 2013, from http://neutrons.ornl.gov/nrsf2/

Pang, J., Holden, T., Wright, J., & Mason, T. (2000). The generation of intergranular strains in 309H stainless steel under uniaxial loading. *Acta materialia, 48*(5), 1131-1140.

Pang, J. W. L., Holden, T. M., & Mason, T. E. (1998). In situ generation of intergranular strains in an A17050 alloy. *Acta Materialia, 46*(5), 1503-1518.

Perry, C. (1969). Plane-shear measurement with strain gages. *Experimental Mechanics, 9*(1), 19N-22N. doi: 10.1007/bf02327879

Pintschovius, L., Jung, V. Macherauch, E.,Shäfer, R., Vöhringer O. (1981, July 1981). *Detemination of internal stress distributions in the interior of tehcnical parts by means of neutron diffraction*.

Post, D. (1991). Moiré interferometry: Advances and applications. *Experimental Mechanics, 31*(3), 276-280. doi: 10.1007/bf02326072

Primm, R. T., Chandler, D. I. G., Jolly, B. C., Miller, J. H., & Sease, J. D. (2008). Design Study for a Low-Enriched Uranium Core for the High Flux Isotope Reactor, Annual Report for FY 2008 Oak Ridge National Laboratory.

Pynn, R. (1984). Neutron scattering instrumentation at reactor based installations. *Review of Scientific Instruments, 55*(6), 837-848. doi: doi:http://dx.doi.org/10.1063/1.1137855

Rajagopalan, S., Little, A. L., Bourke, M. A. M., & Vaidyanathan, R. (2005). Elastic modulus of shape-memory NiTi from in situ neutron diffraction during macroscopic loading, instrumented indentation, and extensometry. *Applied Physics Letters, 86*(8), 081901.

Röntgen, W. C. (1896). ON A NEW KIND OF RAYS. *Science, 3*(59), 227-231. doi: 10.1126/science.3.59.227

Ruud, C. O. (1982). A review of selected non-destructive methods for residual stress measurement. *NDT International, 15*(1), 15-23. doi: http://dx.doi.org/10.1016/0308-9126(82)90083-9

Shull, C. G. (1995). Early development of neutron scattering. *Reviews of Modern Physics, 67*(4), 753-757.

Shute, C. J., Cohen, J., & Jeannotte, D. (1988). *Residual Stress Analysis of Al Alloy Thin Films by X-Ray Diffraction as a Function of Film Thickness.* Paper presented at the Proc. of MRS Conference, Boston MA.

Singh, A. K. (2009). Analysis of nonhydrostatic high-pressure diffraction data (cubic system): Assessment of various assumptions in the theory. *Journal of Applied Physics, 106*(4), 043514-043514-043518.

Smith, D. J., Leggatt, R. H., Webster, G. A., Macgillivray, H. J., Webster, P. J., & Mills, G. (1988). NEUTRON-DIFFRACTION MEASUREMENTS OF RESIDUAL-STRESS AND PLASTIC-DEFORMATION IN AN ALUMINUM-ALLOY WELD. *Journal of Strain Analysis for Engineering Design, 23*(4), 201-211. doi: 10.1243/03093247v234201

Suresh, S., & Giannakopoulos, A. E. (1998). A new method for estimating residual stresses by instrumented sharp indentation. *Acta materialia, 46*(16), 5755-5767. doi: 10.1016/s1359-6454(98)00226-2

Tang, F., & Hubbard, C. R. (2006). Calibration of NRSF2 Instrument at HFIR (Vol. 2006/541): ORNL/TM.

Taran, Y. V., & Balagurov, A. M. (2012). Correction of a neutron diffraction peak shift due to a partial immersion of a gauge volume in an unstressed sample. *Nuclear Instruments and Methods in Physics Research Section A: Accelerators, Spectrometers, Detectors and Associated Equipment, 679*(0), 19-24. doi: http://dx.doi.org/10.1016/j.nima.2012.03.009

Timoshenko, S. (1962). *Elements of strength of materials* (4th ed. Maruzen Asian ed. ed.). Princeton, N.J.: Van Nostrand;.

van Arkel, A. E. (1925). Über die verformung des kristallgitters von metallen durch mechanische bearbeitung. *Physica B, 5*, 208 - 212.

Vogel, S. C., Hartig, C., Lutterotti, L., Dreele, R. B. V., Wenk, H.-R., & Williams, D. J. (2004). Texture measurements using the new neutron diffractometer HIPPO and their analysis using the Rietveld method. *Powder Diffraction, 19*(1), 65-68.

von Mises, R. (1913). Mechanik der festen Körper im plastisch deformablen Zustand. *Göttin. Nachr. Math. Phys., 1*, 582-589.

Wang, X. L., Spooner, S., & Hubbard, C. R. (1998). Theory of the peak shift anomaly due to partial burial of the sampling volume in neutron diffraction residual stress measurements. [Article]. *Journal of Applied Crystallography, 31*, 52-59.

Webster, G. A., & Ezeilo, A. N. (2001). Residual stress distributions and their influence on fatigue lifetimes. *International Journal of Fatigue, 23*, S375-S383.

Wilkinson, A. J., Meaden, G., & Dingley, D. J. (2006). High-resolution elastic strain measurement from electron backscatter diffraction patterns: New levels of sensitivity. *Ultramicroscopy, 106*(4-5), 307-313. doi: DOI: 10.1016/j.ultramic.2005.10.001

Winholtz, R., & Krawitz, A. (1995). The relaxation of residual stresses with postweld heat treatment in a high-performance weld measured with neutron diffraction. *Metallurgical and Materials Transactions A, 26*(5), 1287-1295. doi: 10.1007/bf02670622

Winholtz, R. A., & Cohen, J. B. (1988). GENERALIZED LEAST-SQUARES DETERMINATION OF TRIAXIAL STRESS STATES BY X-RAY-DIFFRACTION AND THE ASSOCIATED ERRORS. [Article]. *Australian Journal of Physics, 41*(2), 189-199.

Withers, P. J., Preuss, M., Steuwer, A., & Pang, J. W. L. (2007). Methods for obtaining the strain-free lattice parameter when using diffraction to determine residual stress. *Journal of Applied Crystallography, 40*(5), 891-904. doi: doi:10.1107/S0021889807030269

Withers, P. J., Turski, M., Edwards, L., Bouchard, P. J., & Buttle, D. J. (2008). Recent advances in residual stress measurement. *International Journal of Pressure Vessels and Piping, 85*(3), 118-127. doi: http://dx.doi.org/10.1016/j.ijpvp.2007.10.007

Woracek, R., Bunn, J., Penumadu, D., & Hubbard, C. (2012). New Approach to Measure Lattice Strains under Torsional Shear Using In Situ Neutron Diffraction for Polycrystalline Materials. *AIP Conference Proceedings*.

Woracek, R., Bunn, J. R., Penumadu, D., & Hubbard, C. R. (2012). Method to determine hkl strains and shear moduli under torsion using neutron diffraction. *Applied Physics Letters, 100*(19), 191904.

Woracek, R., Penumadu, D., Kardjilov, N., Hilger, A., Strobl, M., Wimpory, R. C., . . . Banhart, J. (2011). Neutron Bragg-edge-imaging for strain mapping under in situ tensile loading. *Journal of Applied Physics, 109*(9), 093506.

Young, W. C. (2002). *Roark's Formulas for Stress and Strain* (7th Edition ed.). New York, NY: McGraw-Hill.

Yu, M. (2002). Advances in strength theories for materials under complex stress state in the 20th Century. *Applied Mechanics Reviews, 55*(3), 169-218.

Zandman, F. (1961). Maximum Shear Strain Measurements and Determination of Initial Yielding by the Use of the Photoelastic Coating Technique *Symposium on shear and torsion testing* (Vol. 63rd Annual Meeting Papers, pp. 3-25): American Society for Testing and Materials

VITA

Jeffrey R. Bunn was born in 1984. He graduated from McKenzie High School with honors in 2003. After high school, he attended undergraduate school at The University of Tennessee at Martin (UTM) in West Tennessee for a B.S. degree in Engineering. Between his junior and senior year he took part in a summer internship at Oak Ridge National Laboratory (ORNL) with Dr. Bob LeMaster from UTM. As part of this internship he worked under Dr. Camden Hubbard. Over that summer and an additional summer of internships, Jeff learned a great deal about residual stress measurement through x-ray and neutron diffraction. Upon introduction of Jeff Bunn to Dr. Dayakar Penumadu from The University of Tennessee at Knoxville (UTK) by Dr. Hubbard, Jeff decided to further his studies in D. Penumadu's research group. After one year in the M.S. Program for Civil and Environmental Engineering, Jeff was awarded a National Science Foundation (NSF) grant as part of the Sustainability Through Advanced Interdisciplinary Research (STAIR) program at UTK to directly achieve his Doctorate in Philosophy in Civil and Environmental Engineering. This five year grant allowed Jeff to study not only the diffraction experiments he was previously working on, but to expand his reach to neutron imaging of fuel cells. Jeff's Doctoral research focused mainly on advanced neutron and x-ray techniques for characterization of materials exposed to complex loadings. Jeff completed his Ph.D. in May of 2014.